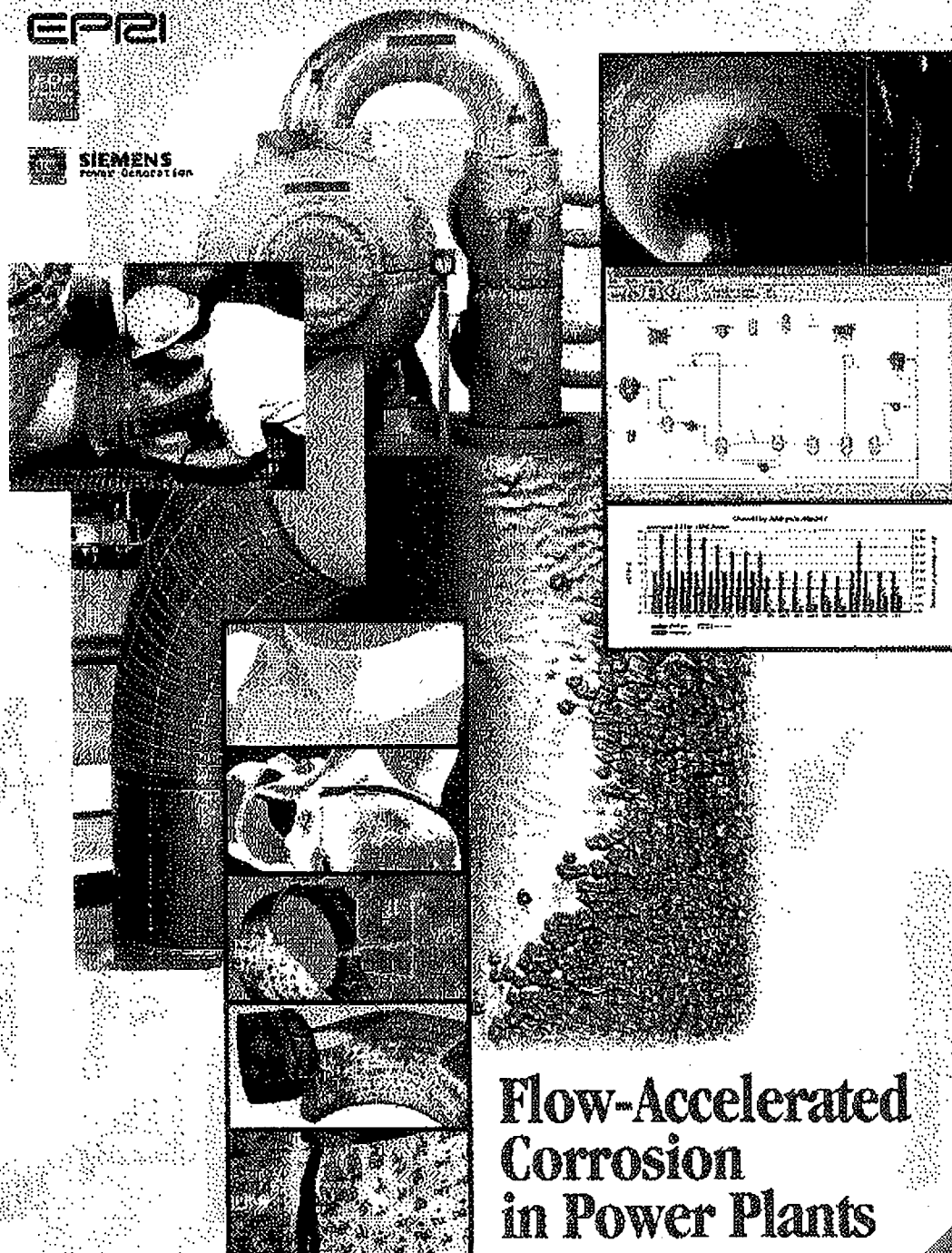


August 12, 2008 (11:00am)

OFFICE OF SECRETARY
RULEMAKINGS AND
ADJUDICATIONS STAFFCORRECTED

Flow-Accelerated Corrosion in Power Plants

U.S. NUCLEAR REGULATORY COMMISSION

In the Matter of Entergy Nuclear Vermont Yankee LLC
Docket No. 50-271 Official Exhibit No. EY-08-04OFFERED by: Applicant/Licensee Intervenor

NRC Staff Other

IDENTIFIED on 7/23/08 Witness/Panel NEC 4Action Taken: ADMITTED REJECTED WITHDRAWNReporter/Clerk MAC

NEC037446

DS-03

Implee Ser-028

FLOW-ACCELERATED CORROSION IN POWER PLANTS

TR-106611-R1

by

Bindi Chexal
Jeffrey Horowitz
Barry Dooley
Peter Millett
Chris Wood
Robin Jones
of
EPRI

Michel Bouchacourt
François Remy
Francis Nordmann
Pierre Saint Paul
of
Electricité de France

Wolfgang Kastner
of
Siemens AG Power Generation

Table of Contents

	Nomenclature	xxxix
1	Introduction to Flow-Accelerated Corrosion	
	Corrosion	1-2
	Flow-Accelerated Corrosion	1-4
	Historical and Technical Background of FAC	1-5
	Laboratory Research	1-5
	Correlation Development	1-6
	Computer Programs To Model FAC	1-6
	Accident at the Surry Power Plant	1-7
	Millstone Accident	1-10
	Pleasant Prairie Power Plant	1-10
	Fort Calhoun Accident	1-12
	Current Global Industry Response	1-12
	References	1-13
2	General Aspects of Corrosion	
	Wall Thinning in Aqueous Systems	2-1
	Wall Thinning Caused by Chemical Effects	2-1
	Wall Thinning Caused by Mechanical Effects	2-4
	Combined Effect of Chemical and Mechanical Processes	2-8
	General Aspects of FAC	2-9
	Conditions Required for FAC	2-9
	Description of the FAC Process	2-10
	Mechanisms of the FAC Process	2-15
	References	2-18
3	Key Parameters Influencing FAC	
	Introduction	3-1
	Factors Influencing FAC	3-1
	Hydrodynamic Factors	3-2
	Environmental Factors	3-13
	Effect of Materials	3-31
	Problems in Modeling FAC	3-36

Table of Contents

Semi-Mechanistic Models for Predicting FAC	3-37
Semi-Mechanistic Models	3-37
CEGB Model	3-50
Investigation of the Semi-Mechanistic Models	3-53
pH Effect	3-53
Mass Transfer Effect	3-62
Temperature Effect	3-78
Effect of Steel Composition	3-85
References	3-97
4 Systems and Components Susceptible to Flow-Accelerated Corrosion	
Commonly Susceptible Systems	4-1
Fluid State	4-1
Operating Time	4-1
Size of Lines	4-2
Nuclear Power Plants	4-3
Power System Flow Diagram	4-3
Piping Systems Typically Susceptible to FAC	4-4
Fossil Power Plants	4-5
Power System Flow Diagram	4-5
Piping Systems Typically Susceptible to FAC	4-8
Differences Between Nuclear and Fossil Plants	4-11
Plant Operating Conditions	4-11
Water Chemistry	4-13
Damage to Other In-Line Components	4-13
Steam Turbines	4-14
Moisture Separator Reheater	4-16
Feedwater Heaters	4-21
Heater Drains	4-27
Steam Generators (Nuclear Plants)	4-27
Fossil Boilers	4-28
Pumps	4-30
Other Notable Problem Areas	4-32
Systems Not Susceptible to FAC	4-33
Plant Experiences with Flow-Accelerated Corrosion	4-34

	FAC in Steam Generators	4-35
	FAC Experience in Piping in the United States	4-43
	FAC Experience in Canada	4-55
	FAC Experience in Europe	4-55
	EPRI's Plant Experience Database	4-73
	References	4-73
5	Water Chemistry Control Practices	
	LWR Water Chemistry	5-1
	Optimization of Water Chemistry for Flow-Accelerated Corrosion	5-6
	PWR Secondary System Chemistry	5-6
	Balance of Plant Considerations	5-7
	U.S. Utility Practices	5-8
	EDF Water Treatments	5-19
	VGB Water Chemistry Guidelines for PWRs	5-22
	Miscellaneous PWR Chemistry Considerations	5-27
	Boiling Water Reactors	5-30
	BWR Chemistry Control for Flow-Accelerated Corrosion (FAC) ..	5-34
	VGB Guidelines for German Boiling Water Reactors	5-37
	Fossil Units	5-41
	United States	5-41
	EDF	5-55
	VGB	5-56
	References	5-61
6	Plant Practices to Detect and Control FAC	
	Introduction	6-1
	Nuclear Plants	6-1
	NUMARC Guidelines	6-1
	NSAC-202L	6-3
	FAC Control Strategies	6-4
	Fossil Plants	6-5
	Typical Utility Tasks to Control FAC	6-7
	Programmatic Aspects of Inspection Programs	6-9
	Inspection Planning	6-10
	Initial Inspection	6-10

Subsequent Inspections	6-11
The Inspection Process	6-12
Ultrasonic Methods	6-12
Radiographic Methods	6-17
Optical Inspection Methods	6-22
New NDE Methods	6-23
Interpretation of Inspection Data	6-29
Actions To Reduce or Eliminate FAC	6-39
Water Chemistry Considerations	6-40
Selection of Pipe Material	6-40
Modification of Operating Conditions	6-45
Local Design Changes	6-46
Qualification of Thinned Components	6-47
Piping Design Codes	6-47
Piping Design Considerations	6-48
Local Wall Thinning	6-49
References	6-52
7 Applications of FAC Prediction Software	
Keller's Model	7-1
Models for Computer Applications	7-4
Software from EDF	7-4
The Siemens/KWU WATHEC and DASY Programs	7-13
The EPRI CHEC Programs	7-19
Software Description	7-36
References	7-44
8 Self-Assessment of Flow-Accelerated Corrosion Programs	
Nuclear Utilities	8-1
Enforcement of FAC Programs	8-2
EPRI Recommendations	8-2
Fossil Utilities	8-5
Enforcement of FAC Programs	8-5
Process Plants	8-5
References	8-6

9 Conclusion

General Aspects	9-1
Key Parameters	9-2
Systems and Components Susceptible to FAC	9-2
Plant Practices to Detect and Control FAC	9-3
Applications of FAC Prediction Software	9-4
Summary	9-4

A Scientific Basis of Corrosion in Aqueous Systems

General Aspects of Aqueous Corrosion	A-1
The Corrosion Cell	A-1
Thermodynamics of Aqueous Corrosion	A-4
Polarization	A-7
Aqueous Corrosion in Alkaline Solutions	A-12
Chemically Stable Species and Oxide Composition	A-12
Behavior of Magnetite Crystals	A-19
The Phenomena of Aqueous Corrosion	A-20
Models of General Aqueous Corrosion	A-21
Corrosion Kinetics	A-23
References	A-28

B Rate Aspects of Wall Thinning

Effect of Velocity on the Rate of Wall Thinning	B-3
Stagnant Water	B-3
Low Velocity	B-4
Critical Velocity	B-4
High Velocity	B-4
References	B-6

C Illustrations of FAC-Induced Wall Thinning**D An Introduction to Fluid Flow and Mass Transfer**

Introduction To Fluid Flow	D-1
Interaction of a Liquid with the Wall of a Flowing System	D-1
Hydraulic Diameter	D-3
Roughness Effect on Turbulent Flows in Pipes	D-6
Dimensionless Approach for Roughness	D-9

Table of Contents

Introduction to Mass Transfer	D-10
Reynolds Number	D-11
Schmidt Number	D-12
Sherwood Number	D-14
Pressure Drop in Components	D-18
Introduction to Two-Phase Flow	D-19
Steam Quality and Void Fraction	D-21
Flow Regimes	D-22
Correlating Void Fraction	D-23
Chexal-Leflouché Void Model	D-23
Void Fraction Behavioral Characteristics	D-24
References	D-30
Glossary	G-1
Index	I-1

List of Figures

- I Chexal's Four Quadrant Known-Unknown Diagram.... p. xvi
- 1-1 Loss of Availability Due to Corrosion of U.S. Nuclear Plants.... p. 1-2
- 1-2 Sample of Surface Damaged by Flow-Accelerated Corrosion.... p. 1-4
- 1-3 Surry Unit 2 Condensate Failure.... p. 1-7
- 1-4 Millstone Unit 3 Heat Drain Failure.... p. 1-10
- 1-5 Failed Pipe from the Feedwater System at the Pleasant Prairie Fossil Power Plant.... p. 1-11
- 1-6 Failed Sweep Elbow from the Extraction Steam System of Fort Calhoun Station.... p. 1-12
- 2-1 FAC in a PWR Drain Line.... p. 2-3
- 2-2 Interactions of Single or Two-Phase Flows with a Solid Surface.... p. 2-4
- 2-3 Liquid Impact Erosion Observed in Copper Alloy Condenser Tubes after 36,000 Hours Operating in a PWR.... p. 2-6
- 2-4 Material Loss Caused by Erosion.... p. 2-7
- 2-5 Typical FAC Superficial Damage Produced in a Very Strongly Reducing Environment (High Purity Feedwater with Cation Conductivity of $\sim 0.1 \mu\text{S/cm}$, Oxygen $< 1 \text{ ppb}$, Hydrazine of $\sim 25 \text{ ppb}$, and an ORP of Approximately -350 mV).... p. 2-10
- 2-6 Scalloped Appearance of Single-Phase FAC (45° Impingement Test at 356°F (180°C) and 184 ft/s (56 m/s) with a pH of 9.0 (at 77°F (26°C)) with Ammonia Water Treatment) as Observed Under a Scanning Microscope.... p. 2-11
- 2-7 Tiger Striped Appearance of Two-Phase FAC.... p. 2-12
- 2-8 Microstructure of Carbon Steel in the Plane Parallel to the Rolling Direction.... p. 2-13
- 2-9 Scanning Electron Microscope Observation Showing the Selective Attack on the Pearlite Phase on a Carbon Steel Surface.... p. 2-13
- 2-10 Scanning Electron Microscope Observation of a Magnetite Cross Section.... p. 2-14
- 2-11 Schematic Representation of the FAC Process.... p. 2-15

List of Figures

- 2-12 Schematic Representation of Oxide Formed on Iron-Based Feedwater Surfaces During Operation with Deoxygenated AVT under reducing conditions (ORP < 0 mV).... p. 2-18
- 3-1 Effect of Flow Rate on Corrosion in Circulating 572°F (300°C) Water of Low Alloyed Steel.... p. 3-3
- 3-2 Schematical Representation of the Change in the Mechanism of FAC as a Function of the Liquid Velocity.... p. 3-4
- 3-3 Effect of Roughness on Mass Transfer.... p. 3-7
- 3-4 Effect of the Dimensionless Roughness on Mass Transfer.... p. 3-9
- 3-5 Processes that May Occur when Steel is Exposed to Contaminated, Flowing Water.... p. 3-14
- 3-6 Influence of Copper Ions in Solution on the Rate of FAC.... p. 3-18
- 3-7 Influence of Copper Ions in Solution on the Rate of FAC.... p. 3-19
- 3-8 Flow and Temperature Dependence of Single-Phase FAC with Ammonia at a pH of 9.04 at 77°F (25°C) (Data Taken Downstream of Orifice).... p. 3-25
- 3-9 Temperature Dependence of Single-Phase FAC Under Neutral Conditions, pH of 7 at 77°F (25°C) (Data Taken on Geometry: Plate Specimens).... p. 3-26
- 3-10 Temperature Dependence of Single-Phase FAC for High and Low Velocity Specimens with Ammonia at a pH of 5.6 at 77°F (25°C) (Data Taken on Inner Surface of Annulus).... p. 3-27
- 3-11 Temperature Dependence of Single-Phase FAC with Ammonia at a pH of 9.0.... p. 3-28
- 3-12 Temperature Dependence of Two-Phase FAC.... p. 3-29
- 3-13 Temperature Dependence of Two-Phase FAC with a Steam Quality of 65% and a Velocity of 185 ft/s (56 m/s).... p. 3-30
- 3-14 Temperature Dependence of Two-Phase FAC.... p. 3-30
- 3-15 Material Dependence of FAC.... p. 3-32
- 3-16 Material Dependence of FAC.... p. 3-33
- 3-17 Material Dependence of FAC for Geometry: Plant Specimens.... p. 3-34
- 3-18 Material Composition Effect on the Magnetite Porosity at 435°F (225°C) with pH of 9.0 Using Ammonia.... p. 3-35
- 3-19 Schematic Representation of the Berge Model.... p. 3-39
- 3-20 Schematic Representation of the FAC Process.... p. 3-40

- 3-21 Schematic Representation of the MIT Model.... p. 3-43
- 3-22 Plot of the Reaction Rate Constant K^* p. 3-46
- 3-23 Scanning Electron Microscope Observations of the Cross Sections of the Oxide Surface on 2 Steel Specimens Exposed to Single-Phase Flow at 355°F (180°C) with pH of 9.0 at 77°F (25°C) using Ammonia.... p. 3-47
- 3-24 Effect of the Oxide Thickness of the FAC Process.... p. 3-48
- 3-25 Effect of the Reaction Rate Constant on the FAC Process.... p. 3-49
- 3-26 Effect of pH on the Rate of FAC for Geometry: Plant Specimens and a Pipe Specimen.... p. 3-54
- 3-27 Effect of pH on the Rate of FAC.... p. 3-55
- 3-28 Scanning Electron Microscope Observations of Ferrite Grains Exposed to Two-Phase Flow in the Five Cail Babcock Loop at 350°F (175°C), with Impinging Flow at 185 ft/s (60 m/s), Steam Quality of 64% at 1700x.... p. 3-56
- 3-29 Scanning Electron Microscope Observations of Pearlite Grains Exposed to Two-Phase Flow in the Five Cail Babcock Loop at 350°F (175°C), with Impinging Flow at 185 ft/s (60 m/s), Steam Quality of 64% at 480x.... p. 3-57
- 3-30 Equilibrium Iron Solubility Dependence of Single-Phase FAC Obtained in the EDF-Ciroco Loop at 355°F (180°C).... p. 3-59
- 3-31 Equilibrium Iron Solubility Dependence of Two-Phase FAC Obtained in the EDF Five-Cail Babcock Loop at ~350°F (~175°C).... p. 3-60
- 3-32 Equilibrium Iron Solubility Dependence of Single-Phase FAC Obtained in the EDF-Ciroco Loop.... p. 3-61
- 3-33 Dependence of Single-Phase FAC Rates on Mass Transfer Coefficient at 300°F (149°C) with a pH of 9.05.... p. 3-64
- 3-34 Mass Transfer Coefficients as a Function of Temperature.... p. 3-65
- 3-35 Mass Transfer Coefficient Dependence of FAC Rates in Single-Phase Flow at 355°F (180°C) and a pH of 9.0 at 77°F (25°C) Using Ammonia.... p. 3-67
- 3-36 Mass Transfer Coefficient Dependence of FAC Rates in Single-Phase Flow at 355°F (180°C) and Using Several pHs.... p. 3-68
- 3-37 Appearance of Test Surface Before the Test (as Received Conditions - Machined and Polished).... p. 3-70

List of Figures

- 3-38 Appearance of Test Surface After Testing Carried Out at 355°F (180°C) with a pH of 9.0 Using Ammonia on a 0.315 inch (8 mm) ID Tube with a Velocity of 12 ft/s (4 m/s) and a Wear Rate of 11 mils/yr (0.03 micron/hr).... p. 3-71
- 3-39 Appearance of a Test Surface After Testing Carried Out at 355°F (180°C) with a pH of 9.0 Using Ammonia on a 0.315 inch (8 mm) ID Tube with a Velocity of 50 ft/s (16 m/s) and a Wear Rate of 121 mils/yr (0.35 micron/hr).... p. 3-72
- 3-40 Appearance of a Test Surface After Testing Carried Out at 355°F (180°C) with a pH of 9.0 Using Ammonia on a 0.157 inch (4 mm) ID Tube with a Velocity of 105 ft/s (34 m/s) and a Wear Rate of 862 mils/yr (2.5 micron/hr).... p. 3-73
- 3-41 Roughness Effect on FAC Rates.... p. 3-74
- 3-42 Steam Quality Dependence of Two-Phase FAC Rates at 345°F (175°C) with pH of 9.0 Using Ammonia.... p. 3-76
- 3-43 Scanning Electron Microscope Views of Oxide Cross Sections After Tests at the EDF Ciroco Loop at 355°F (180°C) with a pH of 9.0 at 77°F (25°C) Using Ammonia.... p. 3-77
- 3-44 Mass Transfer Coefficient Dependence of the FAC Rates in Single-Phase Flow.... p. 3-79
- 3-45 Temperature Dependence of FAC Rates in Single-Phase Flow.... p. 3-80
- 3-46 Scanning Electron Microscope Views of the Surface Appearances After Testing in the EDF Ciroco Loop (Test Duration was Approximately 48 to 60 Hours).... p. 3-81
- 3-47 Scanning Electron Microscope Views of the Surface Appearances After Testing in the EDF Ciroco Loop (Test Duration was Approximately 48 to 60 Hours).... p. 3-82
- 3-48 Scanning Electron Microscope Views of the Surface Oxide Obtained from Plant Samples.... p. 3-84
- 3-49 Scanning Electron Microscope Views Showing the Steel Composition Effect on the Porosity of the Magnetite Layer at 435°F (225°C) with a pH of 9.0 Using Ammonia.... p. 3-86
- 3-50 Profile Analysis Using Glow Discharge Spectrometry on a Steel Specimen Containing 0.025% Chromium, Single-Phase, at 435°F (225°C) with a pH of 9.0 Using Ammonia.... p. 3-87

- 3-51 Profile Analysis Using Glow Discharge Spectrometry on a Steel Specimen Containing 1.54% Chromium, Single-Phase, at 435°F (225°C) with a pH of 9.0 Using Ammonia.... p. 3-88
- 3-52 FAC Rate Dependence on the Steel Composition for Both Single and Two-Phase Flows.... p. 3-89
- 3-53 Scanning Electron Microscope Examination of Carbon Steel, Steam Generator J Tube with a Chromium Concentration of 0.016%.... p. 3-91
- 3-54 Scanning Electron Microscope Examination of Carbon Steel, Steam Generator J-tube with a Chromium Concentration of 0.135%.... p. 3-92
- 3-55 Main Improvement Carried Out in the FAC Model to Take Account of the Chromium Effect.... p. 3-94
- 3-56 Time and Chromium Concentration Dependency of FAC for PWR J-tubes at 221°C and 9 m/s.... p. 3-95
- 3-57 Temperature Dependence of FAC Rates in Single-Phase Flow Obtained in the EDF Ciroco Loop for Several Steels with a pH of 9.0 at 77°F (25°C) Using Ammonia.... p. 3-96
- 4-1 Typical Nuclear Power Plant Heat Balance Diagram.... p. 4-3
- 4-2 Typical Drum Boiler Fossil Plant Cycle Showing Locations of Impurity Ingress, Corrosion and Deposition.... p. 4-7
- 4-3 Typical Once-Through Boiler Fossil Plant Cycle Showing Locations of Impurity Ingress, Corrosion and Deposition.... p. 4-7
- 4-4 Failed Elbow from the Feedwater System at the Navajo Fossil Power Plant.... p. 4-8
- 4-5 Mollier-Diagram Showing Flow-Accelerated Corrosion Zones of Saturated Steam Turbines [4.7].... p. 4-15
- 4-6 Wet Steam Velocities Calculated for the Initial Design of the MSR Used for EDF's 900 MWe PWR Units.... p. 4-17
- 4-7 Damage Caused by Secondary Flow in the MSR of a 900 MWe EDF PWR Unit.... p. 4-18
- 4-8 Damage Caused by the Jet from a Leak in a Reheater Tube in the MSR of a 900 MWe PWR EDF Unit (Steam at 518°F (270°C) and 798 psi (5.5 MPa), Water at 507°F (264°C) and 725 psi (5 MPa)).... p. 4-19
- 4-9 MSR Tube Protection Resulting from a Change in the Water Treatment from Ammonia to Morpholine in a 900 MWe EDF PWR Unit.... p. 4-20

List of Figures

- 4-10 Damage in a Low Pressure Feedwater Heater of a 900 MWe PWR EDF Unit.... p. 4-22
- 4-11 Damage at the Feedwater Heater Inlet of a 900 MWe EDF PWR Unit.... p. 4-23
- 4-12 Theoretical versus Measured Extraction Line Quality.... p. 4-24
- 4-13 Damage Caused by Bypass Flow Around a Baffle in a Low Pressure Feedwater Heater of a 900 MWe EDF PWR Unit.... p. 4-25
- 4-14 Changes in the Design of the Feedwater Heaters of some of EDF's 900 MWe PWR Units.... p. 4-26
- 4-15 Cross Section Through Economizer Inlet Header and Tubes Showing Flow-Accelerated Corrosion in the Tubes.... p. 4-29
- 4-16 Flow Accelerated Corrosion and Burst in Economizer Inlet Header Tubes.... p. 4-30
- 4-17 Material Dependence of Single-Phase FAC Rates Obtained in the Creil Loop of EDF.... p. 4-31
- 4-18 FAC Damage to J-tubes in the Fessenheim Power Plant (a 900 MWe EDF PWR unit).... p. 4-36
- 4-19 FAC Damage to the Feed Rings at the Diablo Canyon Plant.... p. 4-38
- 4-20 Local FAC Damage on the Feed Ring at the Impact Area of Jets from the J-tubes at the Fessenheim Power Plant (a 900 MWe EDF PWR unit)..... p. 4-39
- 4-21 Typical Aspect of Damaged Flow Holes (Nominal Flow Hole Diameter of 19 mm).... p. 4-40
- 4-22 Steam Generator Tube Eggcrate Support Damage at San Onofre Nuclear Generating Station.... p. 4-42
- 4-23 Failed Elbow from the Feedwater System at the Navajo Fossil Power Plant.... p. 4-45
- 4-24 Surry Unit 2 Condensate Failure.... p. 4-46
- 4-25 Location of the Rupture in Surry Unit 2.... p. 4-47
- 4-26 Failed Pipe Downstream of a High Pressure Turbine Nozzle in Unit 2 of the Arkansas Nuclear One Nuclear Station.... p. 4-49
- 4-27 Millstone Unit 3 Heater Drain Failure.... p. 4-50
- 4-28 Millstone Unit 2 Failure in the Reheater Drain System.... p. 4-51
- 4-29 Millstone Unit 2 Failure in the Heater Drain Bypass System.... p. 4-52
- 4-30 Failed Pipe from the Feedwater System at the Pleasant Prairie Fossil Power Plant.... p. 4-53

- 4-31 Failed Sweep Elbow from the Extraction Steam System of Fort Calhoun Station.... p. 4-54
- 4-32 Damage in the Steam Generator of the Saint Laurent Gas Cooled Reactor Power Plant.... p. 4-59
- 4-33 Damage in the Discharge Pipe of a Feedwater Pump at Bouchain Unit 1 (a 250 MWe Fossil Fired Power Plant).... p. 4-60
- 4-34 Damaged Section Between the High Pressure Turbine and the Moisture Separator Inlet at the Belgium Tihange Nuclear Power Plant.... p. 4-61
- 4-35 Damaged Section Between the High Pressure Turbine and the Moisture Separator Inlet at the EDF Bugey Nuclear Power Plant.... p. 4-62
- 4-36 Damage in the Moisture Separator of a CP1 (a 900 MWe PWR Power Plant).... p. 4-63
- 4-37 Arrangement of the High Pressure Feedwater Heaters and High Velocity Separators in the French 1,300 MWe Nuclear Plants.... p. 4-64
- 4-38 Details of the Leak in the Heater Drain System at Bugey (a 900 MWe PWR)..... p. 4-65
- 4-39 Upstream View of the Feedwater Failure at Loviisa (a 445 MWe Finnish PWR).... p. 4-67
- 4-40 Downstream View of the Feedwater Failure at Loviisa (a 445 MWe Finnish PWR).... p. 4-68
- 4-41 Rupture of Extraction Line from a Russian Designed VVER.... p. 4-70
- 4-42 Characteristic FAC Wear Patterns of the Component Shown in Figure 4-41.... p. 4-70
- 4-43 Feedwater Locations Identified as Sensitive to FAC.... p. 4-71
- 5-1 PWR Secondary Chemistry Optimization Diagram.... p. 5-3
- 5-2 PWR Primary Chemistry Optimization Diagram.... p. 5-4
- 5-3 Boiling Water Reactor Water Chemistry Optimization Diagram.... p. 5-4
- 5-4 Implementation of Advanced Water Chemistries in U.S. PWRs.... p. 5-11
- 5-5 Comparison of Amine Feedwater Concentrations Required for pH Control..... p. 5-13
- 5-6 Comparison of Condensate Polisher Loading for Various Alternate Amines..... p. 5-14

List of Figures

- 5-7 Distribution of Amines in Use in U.S. PWRs.... p. 5-15
- 5-8 Evolution of Materials Required for Various Components During the Construction of the EDF's PWRs.... p. 5-22
- 5-9 Sampling Points at PWR Required by VGB Water Chemistry Guidelines [5.15].... p. 5-24
- 5-10 Effects of Normal Water Chemistry, Noble Metals Chemical Addition, and Hydrogen Water Chemistry on FAC.... p. 5-35
- 5-11 Relevant Sampling Points at German BWRs.... p. 5-38
- 5-12 Schematic Representation of Oxide Formed on Iron-Based Feedwater Surfaces During Operation with OT.... p. 5-45
- 5-13 Changes in Oxidizing Reducing Potential (ORP) and Feedwater Iron Levels (Fe) at the Economizer Inlet when Hydrazine (N_2H_4) is Gradually Reduced on a 600 MW Drum Unit with an All-Ferrous Feedwater System.... p. 5-47
- 5-14 Change in Feedwater Iron and Oxygen Levels at the Economizer Inlet Upon Elimination of Oxygen Scavenger (Carbohydrazide).... p. 5-48
- 5-15 Change in Boiler Pressure Drop Increase when Hydrazine is Eliminated and when Oxygen is Injected.... p. 5-49
- 6-1 Fossil Plant FAC Program Road Map.... p. 6-6
- 6-2 Thickness Measurements Using the Pulse-Echo Method.... p. 6-13
- 6-3 Panametrics' 36DL+ Hand Held UT Instrument.... p. 6-14
- 6-4 Sample Component Gridded for UT Inspection.... p. 6-16
- 6-5 Sample Radiograph Showing FAC Degradation in a Pipe Downstream of a Socket Welded Elbow.... p. 6-18
- 6-6 Radiographic Exposure Using the Tangential Beam Approach.... p. 6-19
- 6-7 Radiographic Exposure Using the Perpendicular and the Tangential Beam Approaches.... p. 6-20
- 6-8 Sketch of the Autogrid UT System.... p. 6-25
- 6-9 A Conceptual Sketch Showing Application of the Digital Radiographic System on Piping.... p. 6-26
- 6-10 Schematic of Magnetostrictive System.... p. 6-28
- 6-11 Band Method.... p. 6-31
- 6-12 Area Method.... p. 6-33
- 6-13 Moving Blanket Method.... p. 6-35
- 6-14 Histogram of Wear - Showing No Wear.... p. 6-37

- 6-15 Histogram of Wear - Showing Considerable Wear.... p. 6-38
- 6-16 Histogram of Wear - Showing Some Wear.... p. 6-39
- 6-17 Before and After Weld Overlay.... p. 6-44
- 6-18 High Velocity Separator.... p. 6-46
- 6-19 Wall Thinning Logic Diagram.... p. 6-49
- 6-20 Types Damaged Amenable for Local Thinning Analysis.... p. 6-51
- 7-1 Plot of Wall Thinning Number, W , versus the Sherwood Number, Sh_r p. 7-6
- 7-2 Effect of the Upstream Element on the Geometric Factor of the Downstream Element.... p. 7-8
- 7-3 Computed Wall Thinning of a Piping System with WATHEC Residual Life Expectancy for a Component.... p. 7-16
- 7-4 Assessment of Wall Thicknesses of Components by 3-D Displays with DASY Trending of Wall Thinning out of Examinations from 2 Outages.... p. 7-17
- 7-5 Rough and Detailed Weak Point Analysis with WATHEC & DASY.... p. 7-18
- 7-6 Chexal-Horowitz FAC Model, Impact of Chromium.... p. 7-22
- 7-7 Chexal-Horowitz FAC Model, Impact of Molybdenum.... p. 7-23
- 7-8 Chexal-Horowitz FAC Model, Impact of Liquid Velocity.... p. 7-24
- 7-9 Chexal-Horowitz FAC Model, Impact of Pipe Diameter.... p. 7-25
- 7-10 Chexal-Horowitz FAC Model, Impact of Oxygen Level.... p. 7-25
- 7-11 Chexal-Horowitz FAC Model, Impact of Change in pH.... p. 7-26
- 7-12 Chexal-Horowitz FAC Model, Impact of Using Ammonia or Alternate Amines at a pH of 9 at 77°F (25°C).... p. 7-27
- 7-13 Chexal-Horowitz FAC Model, Impact of Fitting Geometry.... p. 7-28
- 7-14 Chexal-Horowitz FAC Model, Impact of Steam Quality.... p. 7-29
- 7-15 Chexal-Horowitz FAC Model, Impact of Hydrazine Concentration.... p. 7-30
- 7-16 Chexal-Horowitz FAC Model, Comparison Against Laboratory Data.... p. 7-32
- 7-17 Chexal-Horowitz FAC Model, Comparison Against Plant Data.... p. 7-33
- 7-18 Mass Transfer Entrance Effect.... p. 7-35
- A-1 Schematic of Corrosion Reactions of Iron in Acid Solutions.... p. A-2

List of Figures

- A-2 The Pourbaix Diagram for Iron in Water at 77°F (25°C).... p. A-5
- A-3 Schematic of the Helmholtz Double Layer Showing the Inner Helmholtz Plane and the Outer Helmholtz Plane with their Associated Ions.... p. A-9
- A-4 Soluble Ferrous and Ferric Ion Concentrations in Equilibrium with Magnetite Calculated Using Sweeton & Baes [A.13] and Tremaine & LeBlanc [A.14].... p. A-15
- A-5 Concentration of Ferrous and Ferric Ions Relative to the Total Concentration of Iron in a Saturated Solution at 392°F (200°C).... p. A-16
- A-6 pH Diagram for the Iron-Water System at 392°F (200°C).... p. A-17
- A-7 Schematic Representation of the Magnetite Crystal.... p. A-18
- A-8 Models of Carbon Steel Corrosion in High Temperature Water.... p. A-21
- A-9 Parabolic Rate Constants for the Corrosion of Mild Steel Corrosion in Pure Water and Steam.... p. A-25
- A-10 Schematic of the Difference Between a Protective Corrosion Process and Flow-Accelerated Corrosion.... p. A-27
- B-1 Change in the Corrosion and Erosion Mechanisms as a Function of Liquid Velocity.... p. B-2
- B-2 Kinetics of Erosion and/or Corrosion Processes.... p. B-3
- C-1 A 10" (275 mm OD) 90 degree elbow from an MSR gravity drain line exhibiting a scalloped type damage on the extrados.... p. C-1
- C-2 A 10" (275 mm OD) 90 degree elbow from an MSR gravity drain line exhibiting a scalloped type damage on the extrados.... p. C-2
- C-3 A concentric 6" X 14" (170 mm X 355 mm OD) reducer from a heater drain line exhibiting a scalloped surface and general wall thinning.... p. C-2
- C-4 Fabricated 24" (610 mm OD) tee from a low pressure extraction steam line exhibiting a surface damage morphology characterized by sharp edged excavations which are preferentially oriented toward the incoming flow.... p. C-3
- C-5 A concentric 6" X 14" (170 mm X 355 mm OD) reducer from a heater drain line exhibiting a scalloped surface and wall thinning downstream of a backing ring.... p. C-3
- C-6 A section of 6" (170 mm OD) pipe taken from a horizontal portion of an MSR gravity drain line.... p. C-4

- C-7 A 12" (325 mm OD) 90-degree elbow from a high pressure extraction steam line exhibiting areas of both smooth excavation and a textured oxide layer.... p. C-4
- C-8 A 12" (325 mm OD) 90-degree elbow exhibiting longitudinal and circumferential grid line markings used for UT wall thickness measurements.... p. C-5
- C-9 A 12" (325 mm OD) 90-degree elbow from a high pressure extraction steam line exhibiting areas of smooth excavation and tiger striping.... p. C-5
- C-10 A 12" (325 mm OD) 90-degree elbow from a high pressure extraction steam line exhibiting areas of smooth excavation and a textured oxide layer.... p. C-6
- C-11 An 8" (220 mm OD) tee from a heater drain line exhibiting a both a coarse and fine scalloped surface pattern and wall thinning in the branch (outlet) leg.... p. C-6
- C-12 A 12" (325 mm OD) 90-degree elbow from a high pressure extraction steam line exhibiting area of smooth excavation with a glossy black magnetite surface finish.... p. C-7
- C-13 A 24" (610 mm OD) 90-degree elbow from a high pressure extraction steam line exhibiting smooth excavations and tiger striping at small bore branch connections on the extrados of the upstream end.... p. C-7
- C-14 A 24" (610 mm OD) 90-degree elbow from a high pressure extraction steam line exhibiting well defined tiger striping on the intrados of the upstream end.... p. C-8
- C-15 A 24" (610 mm OD) 90-degree elbow from a high pressure extraction steam line exhibiting tiger striping damage at small bore branch connections on the median at the upstream end.... p. C-8
- C-16 A 24" (610 mm OD) 90-degree elbow from a high pressure extraction steam line exhibiting smooth excavations and tiger striping along the median and extrados.... p. C-9
- C-17 A 24" (610 mm OD) 90-degree elbow from a high pressure extraction steam line exhibiting markings for UT wall thickness measurements.... p. C-9
- C-18 A 24" (610 mm OD) 90-degree elbow from a high pressure extraction steam line exhibiting smooth excavations and tiger striping along the median and extrados.... p. C-10

List of Figures

- C-19 A 10" (275 mm OD) 90-degree elbow from a high pressure extraction line exhibiting large areas of smooth excavations along the extrados..... p. C-10
- C-20 A 10" (275 mm OD) 90-degree elbow from an MSR drain line exhibiting irregularly shaped oxide patterns.... p. C-11
- C-21 A 1.5" (48 mm OD) 90-degree elbow from a steam system drain line which discharges to the main condenser.... p. C-11
- C-22 A 10" (275 mm OD) 90-degree elbow exhibiting a glossy magnetite finish with a scalloped area on the upstream end..... p. C-12
- D-1 Moody Diagram of Darcy Friction Factor.... p. D-4
- D-2 The Velocity Distribution in Turbulent Flow.... p. D-6
- D-3 Details of the Three Regimes for Turbulent Flow.... p. D-7
- D-4 Relative Roughness of New Commercial Piping.... p. D-8
- D-5 Simplified Moody Diagram.... p. D-9
- D-6 Development of the Diffusion (Mass Transfer) and Hydrodynamic Boundary Layers.... p. D-13
- D-7 Comparison of the Thickness of the Hydrodynamic and Diffusion Boundary Layers.... p. D-14
- D-8 Flow Regimes in Convective Boiling.... p. D-20
- D-9 Homogeneous Void Fraction.... p. D-21
- D-10 Generalized from Regime Map for Horizontal Two-Phase Flow.... p. D-22
- D-11 First Quadrant Void Fraction Characteristics.... p. D-25
- D-12 First Quadrant Void Fraction Characteristics.... p. D-26
- D-13 First Quadrant Void Fraction Characteristics.... p. D-27
- D-14 Third Quadrant Void Fraction Characteristic.... p. D-28
- D-15 Third Quadrant Void Fraction Characteristic.... p. D-29
- D-16 Third Quadrant Void Fraction Characteristic.... p. D-30

List of Tables

- 3-1 Published Geometric Enhancement Factor Values for Piping Components with Single Phase Flow as Used in Various FAC Models....p. 3-11
- 4-1 Most Important Fossil Plant Areas Experiencing FAC (Results from 1997 Survey of 63 Utilities [4.2])....p. 4-9
- 4-2 Serious Failures in Fossil Plants Since 1982 [4.3])....p. 4-9
- 4-3 FAC Resistant Materials and Applications for Steam Water Cycle Components [4.7]....p. 4-16
- 4-4 Alloy Content of the Materials Shown in Figure 4-17....p. 4-31
- 4-5 History of U. S. Major FAC Experience....p. 4-44
- 4-6 History of EDF FAC Experience....p. 4-57
- 5-1 Recirculating Steam Generator Power Operation (> 5% Reactor Power) Blowdown Sample/Feedwater Sample....p. 5-10
- 5-2 Comparison of Amines....p. 5-17
- 5-3 EDF Feedwater Chemistry Specifications....p. 5-21
- 5-4 Requirements for the Feedwater of Steam Generators at German PWRs Under Continuous Operation....p. 5-25
- 5-5 Requirements for the Steam Generator Blowdown of German PWRs in Continuous Operation....p. 5-26
- 5-6 Requirements for the Water of Steam Generators of German PWRs in Continuous Operation when Conditioned with Sodium Phosphates.p. 5-27
- 5-7 BWR Chemistry Guidelines - Reactor Feedwater/Condensate - Power Operation....p. 5-31
- 5-8 Median Values of Iron and Copper Concentrations for Table 5-7....p. 5-32
- 5-9 Requirements for the Reactor Feedwater and Reactor Water at German BWRs Under Continuous Operation....p. 5-39
- 5-10 Estimated Percentage of Units Around the World Operating with Either Oxygenated or Deoxygenated Feedwater Treatment....p. 5-42
- 5-11 Economizer Inlet-OT Normal Target Values (N) and Action Levels 1, 2 and 3 for Once-Through Units....p. 5-44
- 5-12 Chemistry Limits for Fossil Plant Feedwater Treatments....p. 5-51

List of Tables

5-13	Drum Boiler Water Treatments....p. 5-53
5-14	Estimated Percentage of Drum Units Around the World Operating with the Three Main Boiler Water Treatments....p. 5-54
5-15	Fossil Water Chemistry Specifications....p. 5-55
5-16	Fully Demineralized Feedwater, Continuous Operation....p. 5-57
5-17	Boiler Water of Demineralized Feedwater, Continuous Operation....p. 5-58
5-18	Fully Demineralized Feedwater, Continuous Operation....p. 5-59
5-19	Boiler Water of Demineralized Feedwater, Continuous Operation....p. 5-60
5-20	Steam, Continuous Operation....p. 5-61
6-1	Single Outage Inspection Data....p. 6-36
6-2	Multiple Outage Inspection Data....p. 6-36
6-3	FAC Resistance of Commonly Used Replacement Alloys....p. 6-40
6-4	Post-Weld Heat Treatment Requirements for Chrome-Moly....p. 6-42
7-1	Keller's Geometry Factors [7.1]....p. 7-3
8-1	FAC Program Self-Assessment Questionnaire....p. 8-3
B-1	Summary of Damage Mechanisms (from Poulson [B.2])....p. B-5
D-1	Heat-Mass Transfer Analogy [D.16]....p. D-15

Nomenclature

α	Void fraction
β	Charge transfer coefficient for hydrogen evolution
δ	Oxide thickness
δ_D	Mass transfer boundary layer thickness
δ_h	Hydrodynamic boundary layer thickness
η	Absolute viscosity
θ	Oxide porosity
Θ	Thermal diffusivity
Λ	Thermal conductivity
μ	Dynamic viscosity
μ_L	Liquid dynamic viscosity
ν	Kinematic viscosity
ν_L	Liquid kinematic viscosity
ρ	Density
ρ_L	Liquid density
σ	Specific heat
τ	Shear stress
e	Turbulent eddy diffusivity
a	Constant
A	Cross sectional area

Nomenclature

A	Component enhancement factor in EDF formulation
A	Empirical constant in Equation 3-42
b	Constant = 0, 1, 2, or 3 depending on the degree of hydrolysis of the ferrous ion
b	Constant
B	Empirical constant in Equation 3-42
B	pH dependent coefficient
c	Concentration
c_f	Blasius friction factor
c_{fr}	Blasius friction factor - rough
c_{fs}	Blasius friction factor - smooth
C	Weight of material removed by corrosion
CR	Corrosion rate
C_{eq}	Ferrous ion concentration in equilibrium
$C^{o eq}$	Ferrous ion concentration in equilibrium at standard hydrogen partial pressure
C_o	Ferrous ion concentration at the metal/oxide interface
C_s	Ferrous ion concentration at the surface
C_{∞}	Ferrous ion concentration in the bulk
$Cr\%$	Weight percent of chromium
$Cu\%$	Weight percent of copper
d	Pipe diameter

d_H	Hydraulic diameter
D	Diffusion coefficient of iron in water
D_o	Outside diameter
DR	Magnetite dissolution rate
e	Roughness element height
e^+	Dimensionless roughness height
E	Longitudinal joint efficiency
E	EMF of the corrosion cell at equilibrium
E°	EMF of the corrosion cell at standard conditions
f	Fraction of the oxidized metal converted to magnetite at the metal/oxide interface
f	Darcy friction factor
F	Faraday's constant
$F_{1,2,3,4,5,6,7,8}$	Factors in the Chexal-Horowitz model and the Kastner Model
G	Gibbs Free Energy
h	Material composition
h	Heat transfer coefficient
i_a	Anodic current
i_c	Cathodic current
J	Mass flux
k	Mass transfer coefficient

Nomenclature

k_L	Loss Coefficient
K	Reaction rate constant
K^*	Reaction rate constant
$K_{1,2,3,4}$	Equilibrium constants
K_c	Keller geometry factor
KD	Vapor-liquid distribution coefficient (also known as the vapor-liquid partition coefficient)
K_p	Parabolic rate constant
K_o	Constant in Equation A-35
K_η	Constant in the Keller equation
K_x	Constant in the Keller equation
L	Pipe length
Mo%	Weight percent molybdenum
Δp	Pressure drop
P	Internal pressure
pK	Base disassociation constant
q	Heat flux
Q	Total mass flow rate
Q	Activation energy for a diffusion process
R	Universal gas constant
Re	Reynolds number
Re_L	Reynolds number of the liquid

Re_o	Reynolds number of the orifice
S	Allowable stress
Sc	Schmidt number
Sh	Sherwood number
She	Standard hydrogen electrode
Sh_{fd}	Sherwood number calculated by the Berger & Hau correlation for a straight tube
Sh_{max}	Maximum Sherwood number
Sh_r	Sherwood number - rough
Sh_x	Local Sherwood number
$Size$	Maximum grid spacing
t	Time
t_{aloc}	Local allowable thickness
t_{init}	Initial thickness
t_{max}	Maximum thickness
t_{meas}	Measured thickness
t_{min}	Minimum thickness
t_{nom}	Nominal thickness
t_{pred}	Predicted thickness
T	Temperature
T_{hoop}	Thickness required to withstand internal pressure
V	Molecular volume

Nomenclature

V	Average velocity
V_L	Liquid velocity
W	Wall thinning number
x	Distance
x	Steam quality
X_{crit}	Critical defect size
y	Distance from the wall
y	Coefficient in Equation 6-2
z	Number of transferred electrons

Introduction to Flow-Accelerated Corrosion

Corrosion is the degradation of a material by means of chemical reactions with the environment. Any time a metal's energy is raised above the ground state, it is no longer passive, and will tend to return to a state of lower energy. That is to say, the act of refining ore to create usable metal ensures that the metal is subject to corrosion. There are different types of corrosion that can occur in a variety of situations. Some forms of corrosion are very common; for example, the rusting of steel in moist environments. This book deals with a less familiar form of corrosion known as flow-accelerated corrosion (FAC). This form of corrosion has plagued nuclear and fossil power plants for many years. Although FAC can occur in many different metals, it has been of most concern in the carbon steel portion of the high temperature piping and equipment found in power plants. FAC results in thinning of piping, vessels, and equipment from the inside out, therefore it cannot be detected except by special means.

Flow-Accelerated Corrosion

Flow-accelerated corrosion¹ is a process whereby the normally protective oxide layer on carbon or low-alloy steel dissolves into a stream of flowing water or a water-steam mixture. The oxide layer becomes thinner and less protective, and the corrosion rate increases. Eventually a steady state is reached where the corrosion and dissolution rates are equal and stable corrosion rates are maintained. In some areas, the oxide layer may be so thin as to expose an apparently bare metal surface. More commonly however, the corroded surface exhibits a black color typical of magnetite.

To the naked eye, the damaged surface has a variable appearance. The appearance is often different for single-phase and two-phase conditions. In single-phase flow, often under a small degree of magnification a *scalloped*, *wavy* or *orange-peel* appearance is observed. In two-phase conditions, a condition called tiger striping is often observed (see Figure 1-2). Further examples of damage are presented in Appendix C.



Figure 1-2. Sample of Surface Damaged by Flow-Accelerated Corrosion
(Courtesy of Altran Corporation)

1. In the United States, flow-accelerated corrosion is commonly but incorrectly known as erosion-corrosion. For reasons that will be explained later, the "erosion-corrosion process" is in reality a pure corrosion process that does not have an erosion component. The term "flow-assisted corrosion" has also been used to describe this process.

Damage caused by flow-accelerated corrosion can be characterized as a general reduction of wall thickness rather than a local attack, such as pitting or cracking. Although FAC occurs over a wide area within a given fitting, it is localized in the sense that it frequently occurs over a limited area of a piping fitting due to local high areas of turbulence. In this context, "localized" may mean within several feet (~1 meter) of the fitting or region of turbulence. However, if one fitting is found to be thinned, then most likely there will be others that have also lost material.

A thinned component will typically fail due to overstress from operating pressure, or abrupt changes in conditions such as water hammer, start-up loading, etc. Large fittings may rupture suddenly rather than provide warning of their degraded condition by first leaking.

FAC occurs under both single and two-phase flow conditions. Because water is necessary in order to remove the oxide layer, FAC does not occur in lines transporting dry or superheated steam.

Two-phase FAC has been recognized as a world-wide problem since about 1970. Since the mid-1980s, single-phase FAC has been acknowledged as a major problem in the balance-of-plant and secondary piping of U.S. and foreign nuclear and fossil plants.

Historical and Technical Background of FAC

Since the 1970s, there have been many studies of the mechanisms of flow-accelerated corrosion. This research was carried out principally in France, Germany, and the United Kingdom. The efforts were a combination of laboratory research and attempts to correlate the laboratory results with plant experience.

Laboratory Research

The laboratory work concentrated on developing an understanding of the mechanism of flow-accelerated corrosion. This effort enabled the researchers to describe the corrosion process. In short, the process was found to be a dissolution of the normally protective oxide layer from the metal surface, leading to local thinning of the oxide and a consequent increase in corrosion rates resulting from rapid diffusion through the oxide film. This research identified the fundamental nature of the process and the governing factors such as: fluid temperature, mass transfer (related to the fluid bulk velocity), alloy composition, oxidizing/reducing potential (ORP, related to the dissolved oxygen and reducing agent), fluid pH

level, component geometry and upstream influences, and steam quality. The corrosion process can be viewed as the mass transfer limited dissolution of the oxide into the flowing stream. As such, the important variables are the solubility and porosity of the oxide, the rate of mass transfer to the stream, and the free stream concentration of soluble iron.

Correlation Development

Early attempts were made to reduce the various laboratory results to a form that would be usable by power plant engineers. The appropriate physical and chemical parameters were mathematically fitted to the FAC rate. Such correlations could then be used to predict the rate of flow-accelerated corrosion as a function of plant conditions. The early attempts at correlating the laboratory data and plant experience were not completely successful, but they did suggest ways for better predictions.

Flow-accelerated corrosion is unusual compared to other corrosion processes because of its greater degree of predictability. For most corrosion processes, the rate of wastage cannot be predicted to within an order of magnitude. Early work to correlate flow-accelerated corrosion with system design and operational parameters showed that FAC was reasonably predictable.

During the past several years, successful correlations have been developed by a number of organizations. To be successful, a correlation must predict the rate of corrosion actually occurring in plant systems as well as in laboratory experiments. Recently, these correlations have been incorporated in computer software. Most of this software has been designed for use on personal computers.

Computer Programs To Model FAC

As part of the response to a 1986 FAC-induced failure at the Surry Power Plant, EPRI developed and introduced the CHEC[®] (*Chexal-Horowitz Erosion-Corrosion*)¹ computer program [1.2] in 1987. This was the first implementation of a flow-accelerated corrosion predictive algorithm on a personal computer. Subsequently, EPRI prepared a family of codes with expanded capabilities to calculate the rate of two-phase FAC and to manage the data produced by an inspection program. This family of codes has now been combined into a single computer code called CHECWORKS[™] (*Chexal-Horowitz Engineering-Corrosion WORKStation*) [1.3]. In addition, programs to address both single and

1. At that time, the term erosion-corrosion was used instead of FAC.

two-phase FAC were developed by Electricité de France (EDF) (the BRT-CICERO™ code) and by Siemens/KWU in Germany (the WATHEC™ and DASY™ code). These codes and their correlations are described in later sections.

Accident at the Surry Power Plant

Although power plants throughout the world have been experiencing FAC problems for decades, the rupture of an elbow in the condensate system at the Surry Nuclear Power Plant in 1986 initiated the present U.S. interest in this problem.

The Surry Nuclear Power Plant, located in Gravel Neck, Virginia, consists of two Westinghouse 822 MWe pressurized water reactors (PWRs). On December 9, 1986, an 18-inch elbow in the condensate system of Unit 2 ruptured during a plant transient (Figure 1-3). Four workers were killed and four other workers were severely scalded. Even though the plant was safely shut down, the United States Nuclear Regulatory Commission (NRC) became concerned because it was apparent that safety-related systems can be damaged by failures in non-safety-related pipes. Post-accident inspections of the Unit 1 and Unit 2 piping revealed widespread degradation due to FAC. As a result, 190 components were replaced because of pipe wall thinning at the two units [1.4].

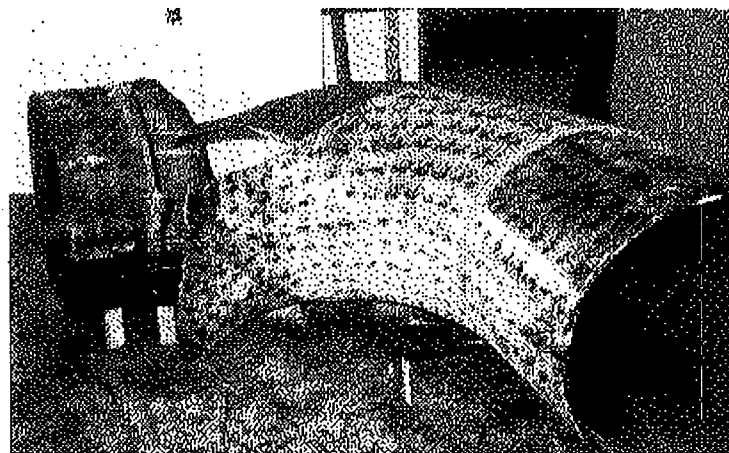


Figure 1-3. Surry Unit 2 Condensate Failure
(Courtesy of Virginia Power)

The Surry accident highlighted the possible consequences of sudden failures that can be caused by FAC. High-energy line breaks are of concern both from safety and economic standpoints. Clearly, a rupture in a high-energy line is a major safety concern. Less obviously, a rupture can damage or actuate safety systems in the area. Finally, failures can result in expensive repairs and purchase of replacement power to offset lost production.

Global Response to the Surry Accident

The unexpected nature and the severity of the Surry accident prompted a quick response from both the U.S. utility industry and the regulatory community. The Surry accident also had implications for foreign nuclear utilities.

The U.S. Industry Response

The initial effort was led by EPRI and by the Virginia Power Company. EPRI sent a letter to all utility chief executive officers of nuclear and fossil power plants providing quick guidance on where and how to look, when to look, and what to do. Virginia Power Company, in parallel, presented detailed briefings on the accident in several locations of the country. The immediate concern was that similar failure potential may exist at other nuclear and fossil power plants. EPRI issued a report titled, "Single-Phase Erosion-Corrosion of Carbon Steel Piping," in February 1987 [1.5]. EPRI also initiated the development of CHEC which was released in July 1987.

In response to the Surry accident, the Nuclear Management and Resources Council (NUMARC)—an umbrella organization¹ that coordinated the nuclear power industry's activities on major issues—formed a working group in April 1987 to address FAC in the nuclear industry. The working group included personnel from utilities, EPRI, and the Institute of Nuclear Power Operations (INPO). Their goal was to formulate an industry approach to flow-accelerated corrosion that would help to prevent further serious failures. The group concluded that large-scale inspection efforts would neither be practical nor necessarily solve the problem. They focused on single-phase FAC because it was felt at the time that degradation of two-phase lines was already adequately addressed by existing utility inspection programs.

The working group recommended a unified industry approach to the issue. This approach included susceptibility analysis combined with a limited number of inspections of components most likely to be affected by FAC. Briefly, the

1. In 1993, NUMARC and several other industry organizations were combined into the Nuclear Energy Institute (NEI).

For the "completely rough turbulent flow" generally found in power plant piping, the roughness height is greater than the laminar boundary layer and is of the same magnitude or greater than the diffusion boundary layer. This indicates that for power plant piping, the Sherwood number will be nearly proportional to the velocity. Thus, FAC will be nearly proportional to velocity.

Effect of Flow Geometry

Both the size and the shape of a component directly influence the velocity and the local mass transfer rate. As one would expect, components with geometries that promote increased velocity and turbulence tend to experience more severe FAC.

FAC is less frequently observed in straight lengths of pipes free from hydrodynamic disturbances. Still, FAC can and does occur in straight piping, especially when the bulk fluid velocity is high. FAC is more often encountered at points of hydrodynamic disturbance, mainly inside and just downstream of fittings in steam and water systems. These include elbows, pipe bends, reducers, tees, at pipe entries, downstream of flow control orifices, valves, etc.

A more detailed discussion of damage locations in both single and two-phase flows can be found in the literature [3.9, 3.11].

A geometric enhancement factor is generally used to represent the effect of increasing turbulence on FAC. The first recognized geometry factors were those from Keller [3.19]. These factors were determined from the experience of FAC in turbines (high wet-steam velocity impingements). When compared to plant data they were not found to be representative of single-phase FAC [3.20].

EPRI has performed extensive studies to correlate different piping geometries with FAC. The resulting, empirically developed, geometry factors [3.21] provide more accurate predictions than were previously available. Some geometry factors are more detailed in that they consider the effect of the upstream configuration on the rate of FAC in the downstream piping [3.22]. In addition, these factors account for FAC, upstream of certain components (e.g. expanders).

Table 3-1 presents a review of geometric factors found in the literature and used to predict FAC [3.19, 3.22, 3.23, 3.24]. The Chexal-Horowitz geometry factors in Table 3-1 are refinements over those previously published earlier [3.22].

Table 3-1. Published Geometric Enhancement Factor Values for Piping Components with Single Phase Flow as Used in Various FAC Models

Fitting	Geometric Factors for FAC				
	Keller [3.19]	Chexal- Horowitz [3.22] + refinements	Remy [3.23]	Woolsey [3.24]	Kastner [3.25]
Straight Pipe [†]	1.0	1.0	1.0	1.0	1.0
90° Elbow	5.75 to 13	3.7	2.1	1.7	6.0 to 11
Reducer (large end) (small end)		2.5 1.8	3.2		
Pipe Entry	4.0			2.5 ²	3.58 to 6.24
Expander (large end) (small end)		3.0 2.8	3.6		
Pipe Expansion				2.0 ²	
Orifice	4.0 to 6.0	5.0	2.9	3.0 to 4.0 ²	
Tee: Flow (run) Combination (branch)	3.74	5.0 5.0	5.7	2.0 to 2.5 ²	
Tee: Flow (run) Separation (branch)	18.75	5.0 4.0	5.7		

1. All the geometry factors are based on comparison with straight pipe.
2. The reference flow is based on the downstream pipe.

Effect of Steam Quality

When the stream flowing past a metal surface is steam and water (two-phase flow), the system pressure (or temperature) and the amount of steam as a mass fraction (the quality) are important. These variables help determine the distribution of voids within the flow at a given cross-section. The ratio of area occupied by vapor to total pipe area at a given cross-section is called the void fraction. The mass

In practice, oxygen-dosed neutral water chemistry and oxygenated treatment for fossil plants use additions of at least 30 ppb of oxygen to the feedwater. These types of water chemistries are used mainly by fossil-fueled plants since oxygen is not tolerated in the boilers of nuclear units [3.29]. (See Chapter 5.)

Metallic impurities. Metallic impurities have a very minor impact on the FAC rate. However, copper, nickel, molybdenum, and lead ions in solution can affect the rate of FAC, even at a feedwater concentration as low as 1 ppb [3.34, 3.35].

The influence of copper appears to be the result of the electrodeposition of Cu^{2+} . This is caused by the negative surface potential formed on surfaces experiencing FAC [3.35]. When this occurs, metallic copper precipitates into the pores of the oxide. As a consequence, oxide porosity and FAC are reduced. The presence of copper ions can be the result of corrosion of copper alloys used in condenser tubes, low pressure heater tubes, etc.

Copper's effects can be important where a high concentration of ammonia is used for the all-volatile treatment (AVT) of the feedwater. Figures 3-6 and 3-7 illustrate data obtained from the CIROCO Loop at EDF using thin layer activation (TLA) corrosion monitoring¹. Figure 3-6 shows the inhibition of corrosion when copper ions are present in the solution. They result from the ammoniated corrosion of copper alloys located in the low pressure part of the feedwater circuit (pH 9.6) and the transport of these ions into the test section located in the high pressure part of the loop. Figure 3-7 shows the increased FAC when the copper alloy tubes are removed and the full feedwater flow passes around a copper tube section using a bypass.

It appears that metallic copper is deposited on the magnetite layer during the high pH operation. When the pH is reduced, the corrosion rate remains low for a period of time apparently due to blockage of the magnetite surface. This result lasted for approximately forty hours until the corrosion rate returned approximately to the original value.

1. The thickness of the activated spot is directly proportional to the count rate. Thus, the corrosion rate, V_c , is equal to the slope of a count rate versus time plot.

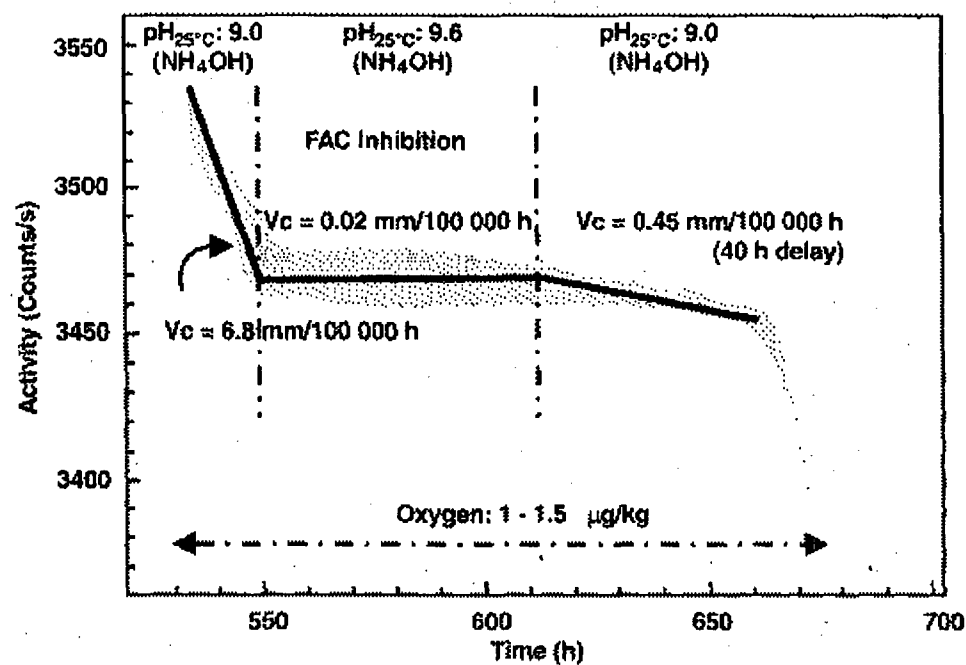


Figure 3-6. Influence of Copper Ions in Solution on the Rate of FAC
(From Bouchacourt [3.36])

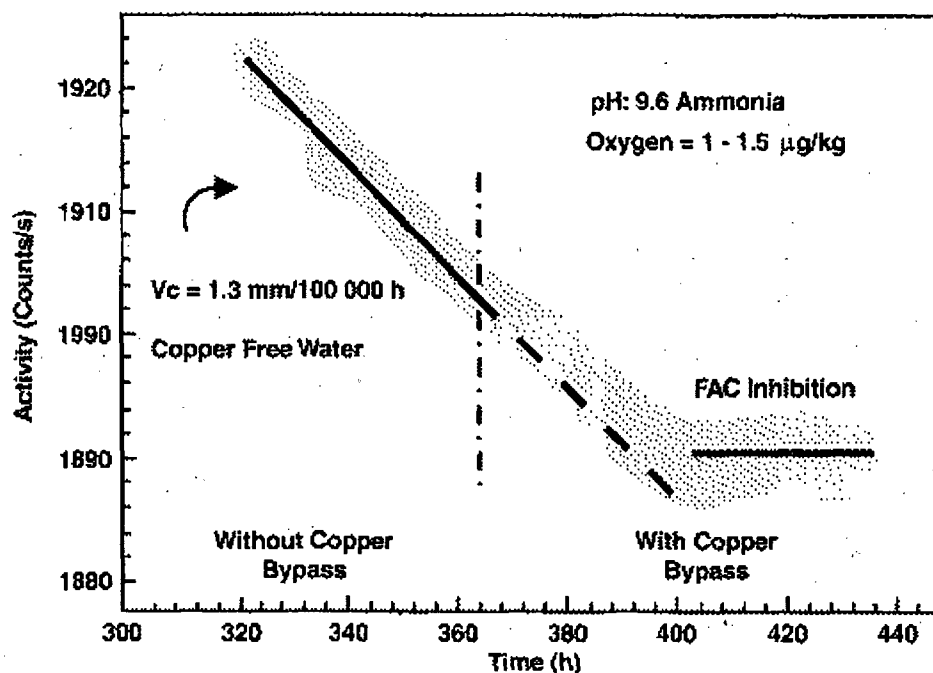


Figure 3-7. Influence of Copper Ions in Solution on the Rate of FAC
(From Bouchacourt [3.19])

An electrodeposition process could explain the presence of other elements such as nickel and molybdenum in the surface oxide layer. It is difficult to rule out the possibility that observed concentrations in the oxide layer are derived solely from the steel [3.35]. Stainless steel is an identifiable source of both nickel and molybdenum in power plant systems.

Deposition of elements such as copper and nickel might eventually lead to complete inhibition of the FAC phenomenon. This depends on the FAC rate and both the concentration and the deposition rates of the metallic ions.

Other impurities. No detailed systematic studies of other water impurities on FAC have been published, probably because most of the laboratory work has been conducted on feedwater with low conductivity. Nevertheless, the presence of low levels of acid forming anions such as Cl^- or SO_4^{2-} has been shown to have no influence on FAC [3.18]. At higher concentrations, if these acidic species are concentrated by an evaporation process, they would be expected to decrease the

pH at the both oxide/water and metal/oxide interface and to promote steel oxidation or the magnetite dissolution process. Two particular circumstances in which one may see increased FAC are:

- The presence of CO_2 caused by air inleakage through condensers or by a thermal decomposition of carbonates or other organic impurities [3.18, 3.33].
- The presence of organic acids such as acetic acid and formic acid generated by decomposition of organic impurities, chemical reagents such as morpholine, ion exchange resins and water treatment additives [3.33].

According to Woolsey [3.24], it is not known whether there are any specific chemical reactions between anion and iron species that would alter the FAC behavior.

Hydrazine

Hydrazine is a reducing agent added to the feedwater/condensate system in a power plant. It is a scavenging agent (removes oxygen), and also maintains a reducing environment in the steam generators (nuclear plants) and in the feed train. Hydrazine is unique in the chemical species in that it is reactive and unstable. It reacts with oxygen forming water and nitrogen. Most of the hydrazine which does not react with oxygen thermally decomposes to form ammonia. Recent information indicates that in the 0-150 ppb range of hydrazine level, the FAC rate increases with increasing hydrazine level as the oxidizing reducing potential (ORP) becomes more reducing. The decrease in potential in this range leads to greater dissolution of the surface magnetite (Fe_3O_4) and thus to an increase in the rate of FAC. Above the 150 ppb hydrazine level, the potential is lowered significantly enough that it leads to slower kinetics. Thus, any further increase in the hydrazine level leads to a decrease in the FAC rate. Therefore, a plot of FAC rate versus hydrazine level is a bell-shaped curve with a peak at 150 ppb.

Theoretical considerations show that the FAC rate should be proportional to the concentration of hydrazine to the 1/6 power. Recent plant and laboratory information shows that this does not continue above 150 ppb of hydrazine.

Hydrazine is commonly added to the feedwater of the PWR secondary circuit to keep feedwater oxygen levels lower than 5 ppb. Hydrazine is used to maintain a reducing environment in the feed train and the steam generator as a scavenger of

Unmonitored FAC damage can be just as dangerous in cogeneration, process plants, and fossil plants as it is in nuclear plants.

Differences Between Nuclear and Fossil Plants

There are significant design and operating differences between nuclear and fossil plants that affect FAC. These are discussed below.

Plant Operating Conditions

Nuclear plants operate with the throttle steam—steam entering the high pressure turbine—saturated, or in the case of plants with once-through steam generators, slightly superheated. In contrast, the throttle steam in modern fossil units is highly superheated and may also be supercritical (above the critical pressure of water).

To understand what this means, it is necessary to compare the power cycles typically used. In both nuclear and fossil stations, condensate leaves the condenser, passes through a number of feedwater heaters, and enters the heat source—boiler, steam generator, or nuclear core. The heat source adds energy to the feedwater, creating steam. The steam leaving the heat source enters the high pressure turbine. Some of the steam flowing through this turbine is removed and used to heat the feedwater. This is known as “extraction steam.” The bulk of the steam exits the high pressure turbine. The condition of the steam at the exit of the high pressure turbine and the downstream equipment are the most important differences between nuclear and fossil steam cycles.

The steam exiting the high pressure turbine in nuclear plants contains significant moisture. This moisture must be removed from the steam before it can enter the lower pressure turbines. Nuclear plants have a moisture separator to remove this moisture and sometimes have a steam heated reheater to superheat the steam. This steam then passes through the low pressure turbine and on to the condenser.

In contrast, the steam leaving the high pressure turbine in a fossil plant is still superheated or only slightly wet. Moisture separators, steam reheaters, and their associated drainage systems are not needed between the high pressure turbine and the lower pressure turbines¹. Most extraction piping in fossil plants carries superheated steam and is thus not susceptible to FAC. Therefore, a fossil unit often does not have the wet steam conditions that contribute to damage in certain nuclear power plant piping systems. However, during start-up and at reduced power levels, steam qualities are lower and some steam systems may be susceptible to FAC. There also may be steam lines directly from the steam drums that have saturated conditions and possibly have some moisture.

The condensate, feedwater, and heater drain systems of fossil and process plants are susceptible to FAC damage. In fact, in fossil plants the areas normally damaged by FAC are between the condensate pump discharge and the boiler entrance and in the heater drains (see the section entitled "Damage to Other In-Line Components" later in this chapter for further information on the type of damage encountered at the entrance to the boiler). Additionally, fossil plants that are used in the peaking mode can also experience FAC-caused damage in the two-phase systems.

Fossil plants can operate as either "base-load" units or "peaking" units. Base-load units operate continuously at high power levels. In this service, operational transients are limited to start-up, shutdown, and equipment malfunctions. Peaking units are started and stopped, or operate at reduced power levels, as needed to meet periods of heavy load demand. Peaking units experience more frequent operational transients than base-load plants.

Peak-load plants are called on to closely follow system load demands and maintain condenser vacuum while in standby mode. By maintaining vacuum, these plants can be on-line in a shorter time than if vacuum had to be re-established. To re-establish a vacuum, the boiler must continuously generate a small amount of steam to operate the air ejectors. While operating in the standby mode, most of the steam-filled portions of a plant operate under conditions that are

1. There is some confusion in nomenclature between nuclear units and fossil units relative to the term "reheaters." In fossil units reheating refers to the practice of routing steam from the high pressure turbine back through the reheating section of the boiler where the temperature of the steam is raised. The steam then is returned to an intermediate pressure turbine.

In nuclear units the reheater is a heat exchanger which heats the steam exiting the moisture separator with diverted main or extraction steam. In the nuclear case, the reheater drains have been an area of FAC problems. No analogous area exists in a fossil unit.

far from normal. There can be high-velocity, two-phase flow in portions of the system that carry superheated steam when at normal power. Peaking units can also operate for substantial periods at reduced power. This also can lead to two-phase flow in lines that carry superheated steam at full power. These modes of operation complicate FAC susceptibility analyses and inspection planning.

Water Chemistry

Modern fossil plants normally use one of several different water treatments [4.4]. Drum boilers typically use all-volatile treatment (AVT), oxygenated treatment (OT), phosphate treatment (PT), congruent phosphate treatment (CPT), or equilibrium phosphate treatment (EPT). Once-through boilers usually use either AVT or OT (see Chapter 5 for further information). Ammonia is the feedwater treatment of choice because it does not break down under the high temperatures experienced in boilers. More complicated amines, such as morpholine, would thermally decompose at boiler temperatures.

As at nuclear plants, hydrazine is often used to produce a reducing feedwater environment, particularly for mixed metallurgy systems, and to remove oxygen from the feedwater. Any hydrazine that enters the boiler is thermally decomposed to form ammonia, hydrogen and nitrogen.

Damage to Other In-Line Components

FAC damage is not restricted to piping and piping components. Any component in the stream is subject to the same corrosion mechanism. The same cause produces the same effects. In general, the most vulnerable areas are where one or more of the following conditions exist:

- The flow has a high velocity.
- There is impingement on a surface.
- There is a large pressure difference that induces internal flows.
- There is a flow with high quality (low moisture) that tends to have a lower concentration of pH control ammonia or amine and consequent decrease in pH.

In evaluating corrosion within equipment, it is necessary to consider the consequences of the damage as well as to know the limit of allowable damage. The engineer should be aware that:

- If there is thinning of internal elements, both the direct and indirect consequences of this thinning should be considered.
- If the wear occurs on a pressure boundary, the engineer must be able to determine if there is sufficient remaining material to withstand the applied load, at least until the component can be repaired or replaced.

To help illustrate the information presented above, some typical experiences with FAC of in-line components will now be described. The items below apply to both nuclear and fossil plants. Note that a detailed presentation of plant-specific FAC events is provided later in this chapter.

Steam Turbines

With regard to damage in steam turbines, two phenomena, flow accelerated corrosion and droplet impingement erosion are particularly noteworthy. This section will briefly discuss wet steam turbines in nuclear power plants and conventional steam turbines in fossil fueled power plants.

The well known bladings damage of the final stages in conventional steam turbines turned out to be comparatively limited in saturated steam turbines in nuclear power plants [4.5]. Experience shows that enlarging the linear blade sizes and increasing the peripheral velocities essentially has positive effects for wet steam turbines. This is connected with the more favorable steam flow of the final stages with the selection of higher condenser pressures dictated by environmental considerations and with the partial load characteristic of the water-separator and superheater.

On the other hand, flow accelerated corrosion has caused considerable wear in unalloyed or low-alloyed steels in wet steam flow exposed parts such as housings, blade series, and shaft seals in the first NPP turbines' early design [4.6].

As a result of steam expansion in the turbine, water is separated out in the wet steam region, which causes the steam flow rate to decrease steadily. Figure 4-5 shows the expansion curve for a saturated steam turbine with external moisture separation and steam reheat contrasted with that of a non-reheat turbine; the endangered areas in which flow-accelerated corrosion tend to occur are depicted. As can be seen, the expansion of reheated steam takes place in a region less

Fort Calhoun Station

On April 21, 1997, with the Fort Calhoun Station (owned by the Omaha Public Power District) reactor operating at a nominal 100% power, the third elbow downstream from the turbine in the extraction steam line ruptured (Figure 4-31). Fort Calhoun Station is a 478 MWe PWR. The elbow was constructed of 12-inch bent pipe with a radius to diameter ratio of 5. The "fish-mouth" rupture was approximately 54 inches long and 18 inches wide. This elbow was located behind several non-safety related Motor Control Centers (MCCs). The event was further complicated by the activation of the sprinkler system within the turbine building. An additional personnel safety issue resulted from damage to some asbestos insulation, resulting in the need to restrict access to the turbine building due to contamination.

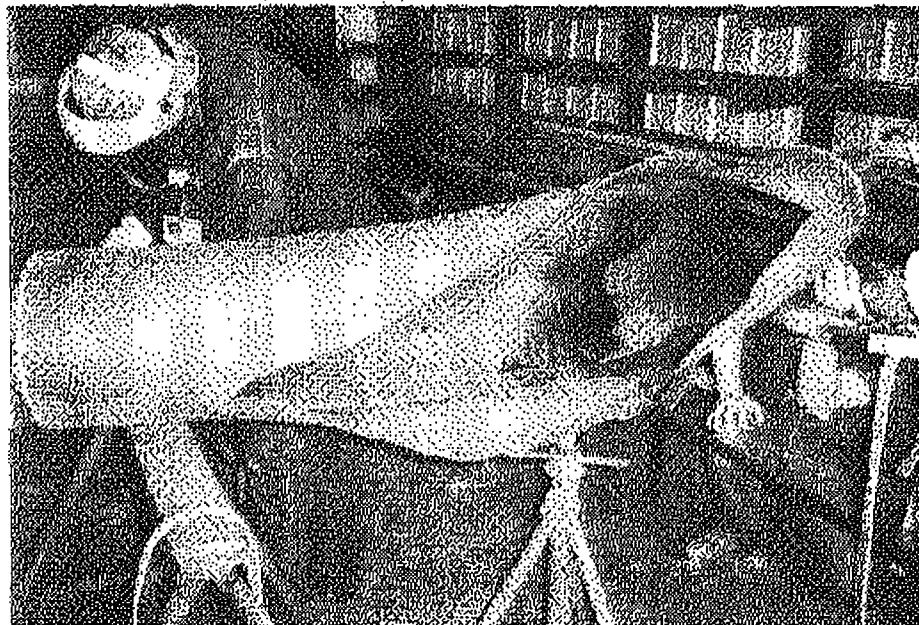


Figure 4-31. Failed Sweep Elbow from the Extraction Steam System of Fort Calhoun Station

(Courtesy of Omaha Public Power District)

Assessment of the pipe rupture indicates that it resulted from excessive pipe wall thinning caused by Flow Accelerated Corrosion (FAC). The pipe thinning occurred over a relatively long period of time, and significant thinning should have been detected well before the event occurred. The site had not been inspected.

Fort Calhoun Station has an FAC control program, however, there was not a detailed, step by step methodology for the process of selecting inspection sites. Such a methodology would define the susceptibility evaluation process and identify situations that would require expansion of the selected inspection locations.

The rupture location was in a system that had been categorized as "susceptible" to FAC and had been incorporated into the EPRI CHECWORKS analytical model, but had not been selected for inspection under the FAC control program. Other sites in this line were inspected, including several shorter radius elbows, a tee, and a reducer. These components had shown expected rates of wear.

The section of piping immediately upstream of the rupture site was replaced in 1985 to address FAC wear of the piping. This indicates that the rupture site would have been an appropriate candidate for inspection.

FAC Experience in Canada

In addition to problems in BOP systems, CANDU plants have experienced FAC in the primary system. CANDU plants are of a pressure tube design with heavy water as a coolant and moderator. Other than the pressure tubes, and the steam generator tubes, the system is constructed out of carbon steel. At the outlet of each pressure tube, there are several fittings and pipes leading up to the outlet header. These fitting have experienced FAC in several CANDU plants. This experience is unusual for several reasons, namely: the temperature is very high 590°F (310°C), the velocities are very high (33-59 feet per second (10-18 m/s)), and the fluid is heavy water.

To ensure against excessive future thinning, the plant operators are conducting increased inspections and investigating water chemistry remedies [4.22].

FAC Experience in Europe

In addition to the experience of the U.S. power plants, there have been significant problems with FAC elsewhere throughout the world.

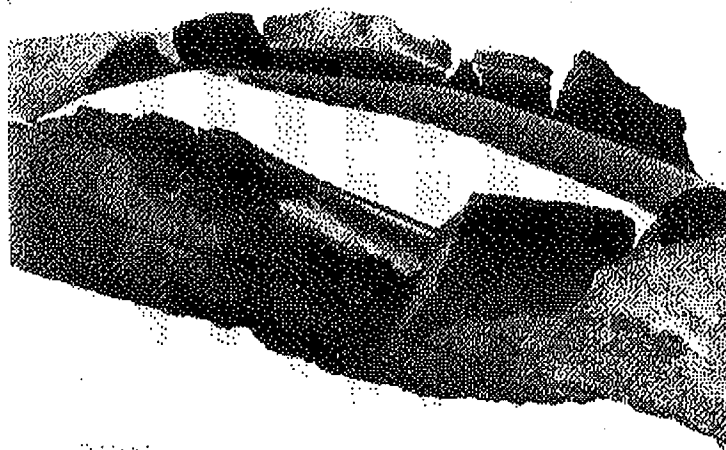


Figure 4-41. Rupture of Extraction Line from a Russian Designed VVER
(Courtesy of Nuclear Research Institute)

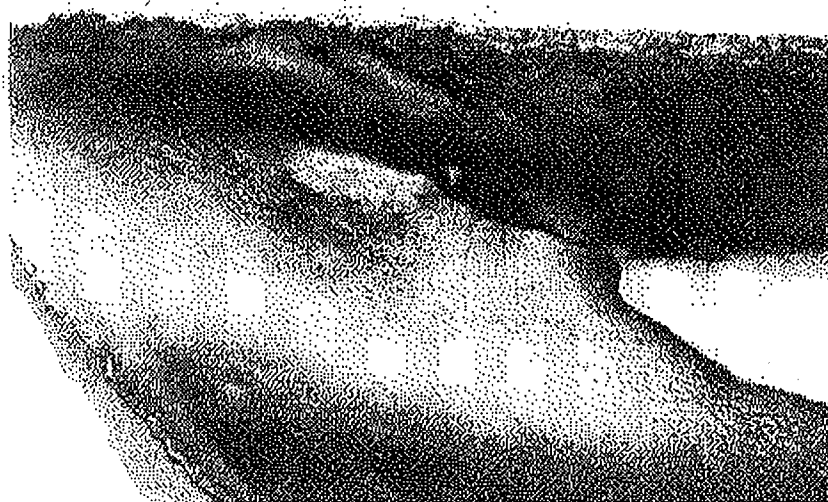
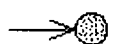











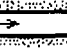





Figure 4-42. Characteristic FAC Wear Patterns of the Component Shown in Figure 4-41
(Courtesy of Nuclear Research Institute)

Table 7-1. Keller's Geometry Factors [7.1]

FLOW PATTERN			REFERENCE VELOCITY	K_c
Primary Flow Stagnation Points		At Pipes	Velocity of Initial Flow (Upstream of Stagnation Obstacle)	1.00
		At Blades		1.00
		At Plates		1.00
		In Pipe Junctions		0.75
				0.60
Secondary Flow Stagnation Points		R/D = 0.5	In Elbows	0.52
		R/D = 1.5		0.30
		R/D = 2.5		0.23
		Behind Pipe Joints	Flow Velocity	0.15
				
Stagnation Points Due to Vortex Formation		Behind sharp edged entrances	Flow Velocity	0.16
		At and behind barriers		0.16
No Stagnation Points		In straight pipes	Flow Velocity	0.04
		In loose horizontal turbine seals	Velocity Calculated from Pressure Drop	0.08
Complicated Flow Through Turbines		In turbine gland seals	Velocity calculated from pressure drop	0.08
		At and above turbine blades and at drainage collecting rings	Average circumferential blade velocity	0.30

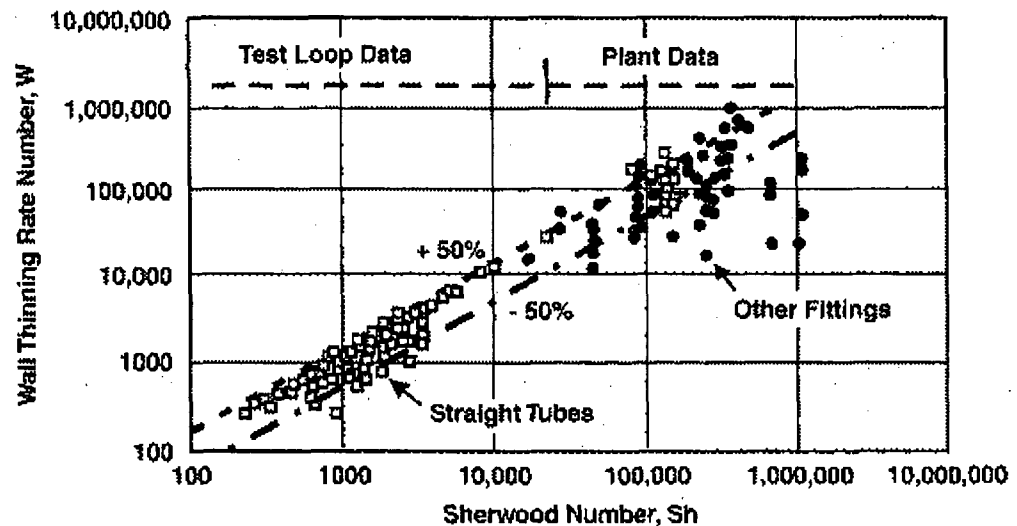


Figure 7-1. Plot of Wall Thinning Number, W , versus the Sherwood Number, Sh ,

(From Bouchacourt [7.3])

The CIROCO loop test results were obtained on straight tubes (OD ~0.31 inches (8 mm)) with Reynolds numbers between 3×10^4 and 2×10^5 . Ammonia or morpholine water treatments (cold pH between 8.8 and 9.6), and a temperature range of 300° to 480°F (~150°C to 250°C) were used. The plant measurements were made on straight, corroded pipes. The thinning rates were large enough to have caused obvious wear in the straight portion of the pipes. The temperature was between 355° and 435°F (~180°C and 225°C), and the cold pH was 8.8.

In addition to validating the assumption of equal Sherwood number and wall thinning rate number, this figure shows two interesting results:

- The thinning is directly proportional to time, as evidenced by comparing results of laboratory tests of 200 hour duration with plant results after 60,000 hours of operation.
- As a direct consequence of the above conclusion, there is no incubation period present in the wear mechanism, i.e. the wear rate is always independent of time.

When several mass transfer correlations were examined, the Reynolds number exponent was between 0.6 and 0.8. This difference corresponds to an uncertainty of $\pm 20\%$ in predicting mass transfer which contributes to the overall wall thinning rate uncertainty of $\pm 50\%$.

The discussion above refers only to straight pipes. But FAC damage appears first in pipe components. In components, there are no general correlations to deduce the mass transfer from hydraulic conditions. To obtain data in components, the same correlation used for a straight tube is used with an enhancement factor, A . The enhancement factor depends on the type of component. More generally, the relationship between the Sherwood number and the wall thickness rate number can be written as:

$$W = A \cdot Sh_r \quad (\text{eq. 7-5})$$

where:

A is the geometry factor.

The value of the enhancement factor was obtained from thickness measurements recorded at plants operated by EDF and other utilities. The chromium content for each data point was estimated from samplings of 200 fittings at EDF plants, and was approximated by the operators at non-EDF plants. Generally, no chromium data exists for the inspected components.

It is clear that the behavior of each component is somewhat different. Part of this discrepancy is caused by uncertainties in the experience feedback analysis such as unknown initial thicknesses and chromium concentrations, uncertainties in wall thickness measurements, actual water chemistry experienced (mainly in the oldest data), and the time of full power operation. To take into account the range of possible predictions, three parameters are defined: the mean, the range, and the maximum. The mean value is considered the most probable and is used in BRT-CICERO to predict the wear rate of other components or for the same component under different conditions. The range is given by the standard deviation of the dispersion. The range is used for the analysis of inspections to conclude if the measured value agrees with the previous value. The maximum value of A gives the most conservative result for evaluating the mechanical behavior of the components.

EDF maintains a database of measured enhancement factors. Included in this database are data for straight pipes, elbows, tees, pipe downstream of regulating valves, orifices, and diffusing sections. The maximum value of A is less than ten and generally is between three and seven.

In addition to the empirical methods of determining A , theoretical methods can be used to estimate A by taking into account the specific geometry of the component. For elbows, the value of A depends on the turning angle and the curvature of the elbow. The wear rate in a tee depends on the velocity ratio of the main to the branch and on the angle of the lateral pipe to the main run. The geometry factor also considers the effect of the upstream component on the downstream component as presented in Figure 7-2.

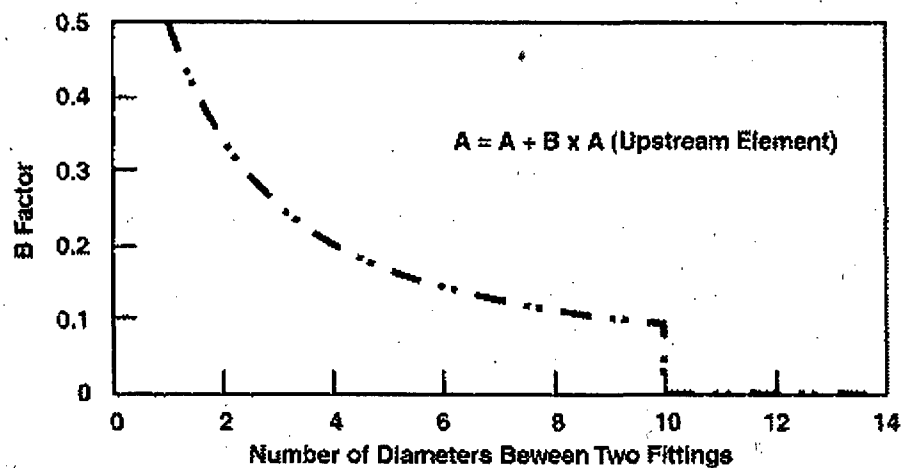


Figure 7-2. Effect of the Upstream Element on the Geometric Factor of the Downstream Element
(From Bouchacourt [7.3])

BRT-CICERO software was designed and developed by the Engineering and Construction Department of the Power Engineering Division of EDF. It is a complete methodology to deal with flow-accelerated corrosion. It is designed to:

- Be comprehensive
- Be conservative
- Optimize the design margin available
- Be both an inspection optimization and a design tool

BRT-CICERO software is composed of two parts. The first part, "Plant Piping Inventory," characterizes the plant systems and their available margins. The second part performs analyses and is designed for use by plant operators. It also uses the data logger files that are produced when performing non-destructive evaluation (NDE) thickness measurements.

Plant Piping Inventory

The system characterization is performed by engineering staff on a mainframe computer using computer aided drafting (CAD) and stress analysis software. The EDF procedure consists of the following three steps:

1. All systems in the plant are classified as being susceptible, or not susceptible to FAC. By considering all of the systems in the plant and eliminating only the ones that are not susceptible, the engineer minimizes the chances of omitting a susceptible line. Systems are excluded from the evaluation for reasons of material, lack of operating time, or for being a small bore line (2 inches (50 mm) or less). The resulting, large-bore susceptible lines are modeled from the available isometric drawings on a CAD system. All available mechanical data such as design conditions, steel grade, code of construction, etc., are included in the database.
2. The next step is to calculate the available structural margin for each component. The first part of this process is to determine whether the pressure stress (the hoop stress) is the governing load. If not, the minimum allowable thickness will be greater than the hoop stress allowable thickness. The design thickness is then compared with an estimated initial thickness obtained by considering the design documentation, the nominal thickness and manufacturing process used. The initial design margin is the difference between the estimated initial thickness and the design thickness. If the initial design margin is too small, additional analyses can be used to compare the local stress level in the thinned area. If the area where the stress level is high does not coincide with the worn area, the thickness loss does not affect the design stress level. For small values of thinning (less than 10% of the nominal thickness), generic calculations are performed for standard components such as elbows, reducers, etc., in order to take advantage of this additional margin from the beginning of operation. Details of this process are explained subsequently. The result of the second step is the identification of the margin available for FAC damage for each component.
3. The third step is to perform the first FAC calculation for each plant using plant specific thermal-hydraulic data and the normal water treatment. The goal of this calculation is to identify groups of components which have

General Plant Diagnosis

During the rough analysis, a plant system list is established that contains information regarding operating conditions of all safety related plant systems. The systems in the list are evaluated by WATHEC to indicate whether they can be disregarded from further analysis. If system operating conditions indicate that a system may be subject to FAC, a detailed analysis is initiated, again using WATHEC.

Detailed Plant Diagnosis

The detailed analysis is thus limited to those lines that are susceptible to FAC and may therefore jeopardize safety. The detailed analysis requires input data on system operating conditions, system design criteria, and the geometric arrangement of piping elements. The program computes the minimum life expectancy for piping components by considering local stress conditions. Based on these values, inspection deadlines are determined. If an evaluation indicates a high risk of piping failure, an NDE examination is scheduled for the next outage.

NDE Wall Thickness Measurement

The PC program DASY handles the storage, administration, evaluation and documentation of wall thickness measurements on individual piping elements. Since the programs WATHEC & DASY have compatible data formats, NDE results are made available to WATHEC and can be used to "calibrate" the predicted susceptibility for all components considered. Additionally, this data allows the elimination of inaccuracies included with input parameters, e.g. true material composition (content of Cr, Cu, Mo of piping elements) or no exact original thickness measurements of components.

Actions to Prevent Flow-Accelerated Corrosion Damage

If significant degradation by flow-accelerated corrosion is detected, an assessment is performed to avoid a safety risk. Assessments may call for periodical checks on piping component wall thickness (monitoring) using WATHEC inspection deadline recommendations. Other options are component repair or replacement or changes in operating conditions. The effectiveness of options proposed can be checked with WATHEC before implementation.

The EPRI CHEC Programs

The CHEC computer program [7.18] was the first of the CHEC series to use the Chexal-Horowitz flow-accelerated corrosion model developed by EPRI in 1987 in response to the Surry accident. The model is empirical and a "best fit" of all data

available [7.19, 7.20]. The model was modified in stages and incorporated in CHECMATE [7.21] and CHECWORKS [7.22] (Chexal-Horowitz Engineering Corrosion Workstation), the most current in the CHEC series of computer programs. The latest version of the Chexal-Horowitz flow-accelerated corrosion model is provided in CHECWORKS.

Chexal-Horowitz FAC Model

Provided below is a description of the model used to predict the rate of single-phase and two-phase flow accelerated corrosion which depends on a large number of interrelated factors. These factors can be divided into three groups: (1) water chemistry variables—pH, dissolved oxygen, hydrazine concentration, and the pH control amine; (2) hydrodynamic variables—fluid velocity, pipe diameter, temperature, steam quality, and the geometry of the flow path; and (3) material variables—percentage of chromium, molybdenum and copper in the steel. The model was developed by correlating:

- All pertinent British, French and German laboratory data
- Assembled U.S. plant data
- EPRI-sponsored tests in support of model development.

The general formulation of the Chexal-Horowitz model is as follows:

$$CR = F_1(T) \cdot F_2(AC) \cdot F_3(MT) \cdot F_4(O_2) \cdot F_5(pH) \cdot F_6(G) \cdot F_7(\alpha) \cdot F_8(H) \quad (\text{eq. 7-7})$$

where:

CR is the FAC rate,

$F_1(T)$ is the factor for temperature effect,

$F_2(AC)$ is the factor for alloy content effect,

$F_3(MT)$ is the factor for mass transfer effect,

$F_4(O_2)$ is the factor for oxygen effect,

$F_5(pH)$ is the factor for pH effect at temperature,

$F_6(G)$ is the factor for geometry effect,

$F_7(\alpha)$ is the factor for void fraction, and

$F_8(H)$ is the factor for hydrazine concentration.

Since the interrelationship between the parameters F_1 through F_8 was not initially apparent, the formulation was developed empirically. In doing so, the following principles were upheld:

- All of the above parameters were incorporated into the model.
- All of the collected data were used in the model development.
- The model did not presuppose a form for the correlation.
- Although the model is empirical, steps were taken to ensure that each part of the model made mechanistic "sense" using EPRI in-house corrosion experience.

Using these principles, an iterative procedure was used until an optimum model was obtained. This model included all of the experimental trends, and correlated well with the bulk of the laboratory data.

The model was further refined by comparing its predictions with actual wear data obtained from nuclear power plants and with additional laboratory data. The use of these additional data (particularly to take into account various geometrical mass transfer enhancement factors) further improved the model. It is worth noting that the FAC rate goes to zero if any of these factors becomes zero. This is the situation when stainless steel is used, where $F_2(AC)$ approaches zero for high amounts of chromium in the alloy. Each of these factors is discussed below.

Temperature Factor. Fluid temperature influences several variables. The variation of FAC rate with temperature is a bell shaped curve with the maximum around 300°F (150°C). The FAC rate is controlled by oxide dissolution kinetics at low temperatures and by mass transfer limitations at high temperatures. The reason for this behavior is believed to be due to the competing behavior of three separate mechanisms in the temperature range of interest (about 200-500°F (~100-250°C)):

1. The solubility of the oxide layer decreases with increasing temperature above 300°F (150°C) and the flow-accelerated corrosion phenomena is mass transfer controlled.
2. The kinetics of the dissolution rate increases with increasing temperature below 300°F (150°C) and the flow-accelerated corrosion phenomena is partially kinetics controlled.
3. The hot pH of an aqueous solution of a pH control agent decreases with temperature in the temperature range of interest.

These three competing effects may explain the shape of the temperature dependency curve.

Alloy Factor. The alloy factor used was a modified form of the Ducreux [7.23] correlation. This correlation relates the flow accelerated corrosion rate with the presence of three alloy elements: chromium, copper, and molybdenum. The substantial decrease in the rate of FAC with even small amounts of chromium is due to the increase of stability of the oxide layer. Chromium tends to reduce drastically the solubility of iron oxides in pure water and thus its presence greatly reduces the FAC rate. The dependence of the predicted FAC rate on the amount of chromium and molybdenum are presented in Figures 7-6 and 7-7.

Geometry Factor. The EPRI geometry factors are more detailed in that they consider the effect of the upstream component on FAC in the downstream piping. In addition, these factors account for FAC upstream of certain components (e.g. expanders). They have been refined over time with additional data and are used in the CHECWORKS code.

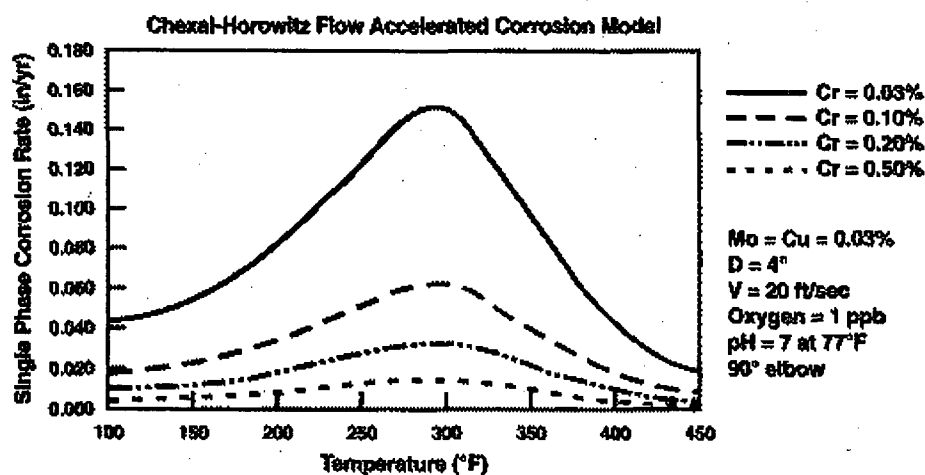


Figure 7-6. Chexal-Horowitz FAC Model, Impact of Chromium

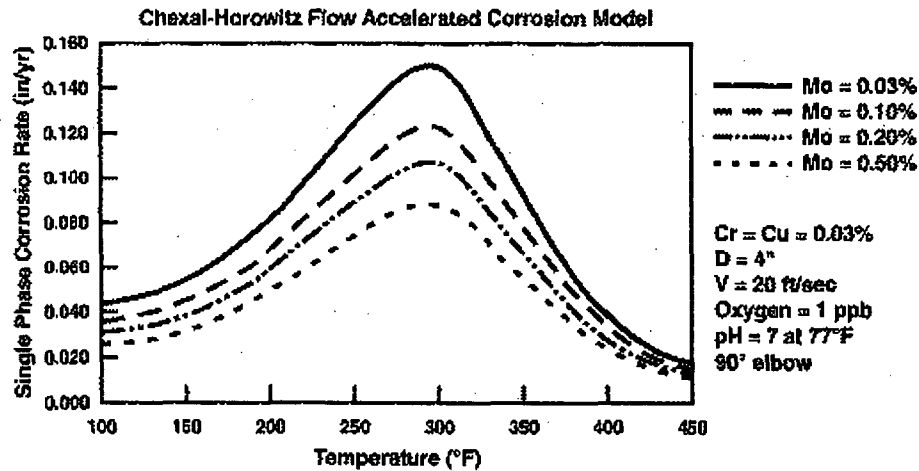


Figure 7-7. Chexal-Horowitz FAC Model, Impact of Molybdenum

Mass Transfer Factor. The mass transfer coefficient is one of the key factors that affects both single-phase and two-phase flow-accelerated corrosion rate. The value of the mass transfer coefficient, k , varies with the local hydrodynamic conditions. Its dependence is expressed in dimensionless form using the corresponding Sherwood number.

$$F_3(MT) \propto k$$

where:

k is $Sh \cdot D / d_H$,

d_H is the hydraulic diameter, and

D is the diffusion coefficient for iron in solution,

and the Sherwood number is determined by:

$$Sh = a \cdot Re^b \cdot Sc^c \quad (\text{eq. 7-8})$$

where:

Re is the Reynolds number ($Re = Vd_H/\nu$),

Sc is the Schmidt number ($Sc = \nu/D$),

V is the liquid velocity,
 ν is the kinematic viscosity, and
 a, b, c are experimentally determined constants.

For two-phase flow the Reynolds number, Re , is based on the velocity in the liquid layer given by,

$$V = \left(\frac{Q}{A \cdot \rho_L} \cdot \frac{1-x}{1-\alpha} \right) \quad (\text{eq. 7-9})$$

where:

Q is the total mass flow rate,
 A is the pipe flow area,
 x is the steam quality,
 ρ_L is the liquid density, and
 α is the steam void fraction.

The dependence of the predicted FAC rate on the liquid velocity and the pipe diameter are presented in Figures 7-8 and 7-9.

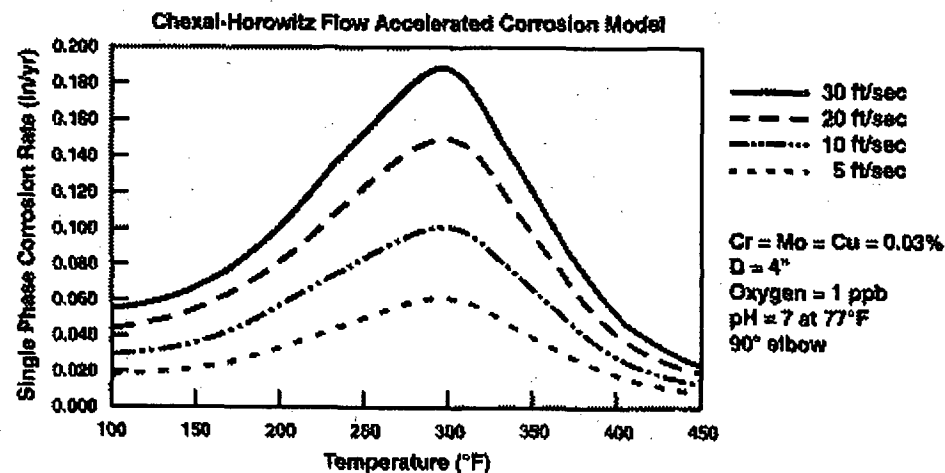


Figure 7-8. Chexal-Horowitz FAC Model, Impact of Liquid Velocity

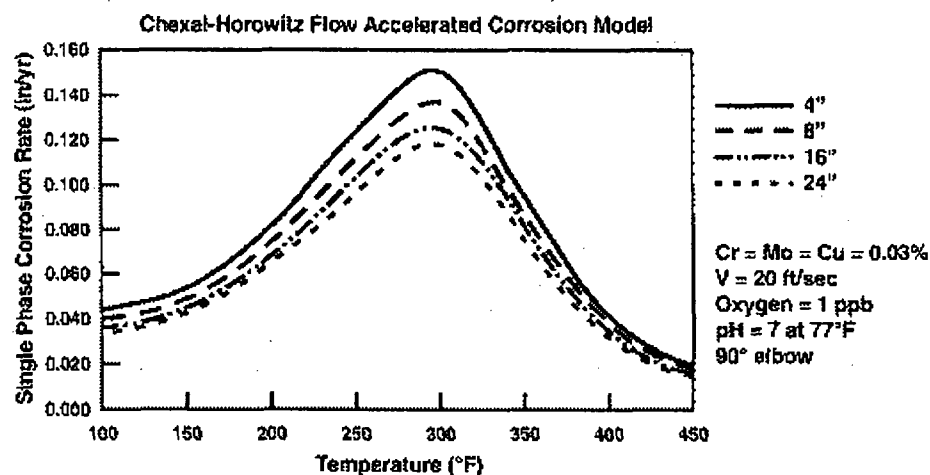


Figure 7-9. Chexal-Horowitz FAC Model, Impact of Pipe Diameter

Oxygen Factor. It has been observed widely in flow-accelerated corrosion that the rate of corrosion varies inversely with the amount of dissolved oxygen present. Data from various sources were correlated and used to develop the oxygen factor used in the Chexal-Horowitz model. The dependence of the predicted FAC rate on the dissolved oxygen is presented in Figure 7-10.

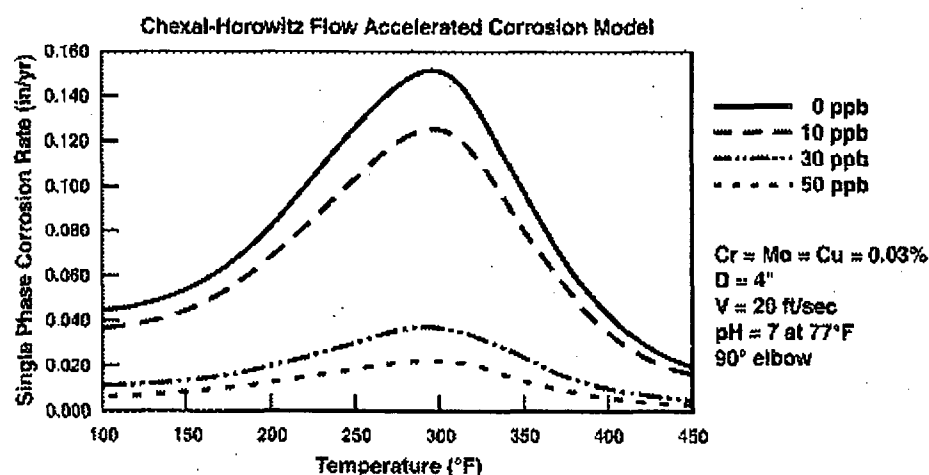


Figure 7-10. Chexal-Horowitz FAC Model, Impact of Oxygen Level

pH Factor. The rate of metal loss is strongly dependent upon the solubility of ferrous ions at the metal surface. One of the main parameters controlling the solubility of iron is the operating temperature pH in the aqueous phase at the oxide-solution interface. The value of pH at operating temperature is calculated by the solution of several non-linear simultaneous equations involving mass balance, charge balance, dissociation constants for water, base dissociation constants and partitioning coefficients of the relevant alkalizing agents and anions. The pH factor used in the model is based on the pH at the operating temperature. This means that the flow-accelerated corrosion rate is a function of amine type, amine concentration and temperature. The dependence of the predicted FAC rate on the condensate pH and the pH control amine are presented in Figures 7-11 and 7-12.

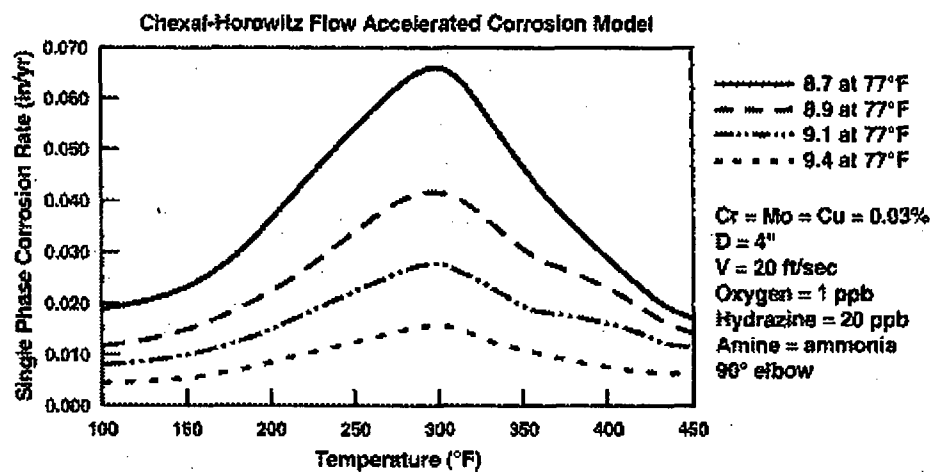


Figure 7-11. Chexal-Horowitz FAC Model, Impact of Change in pH

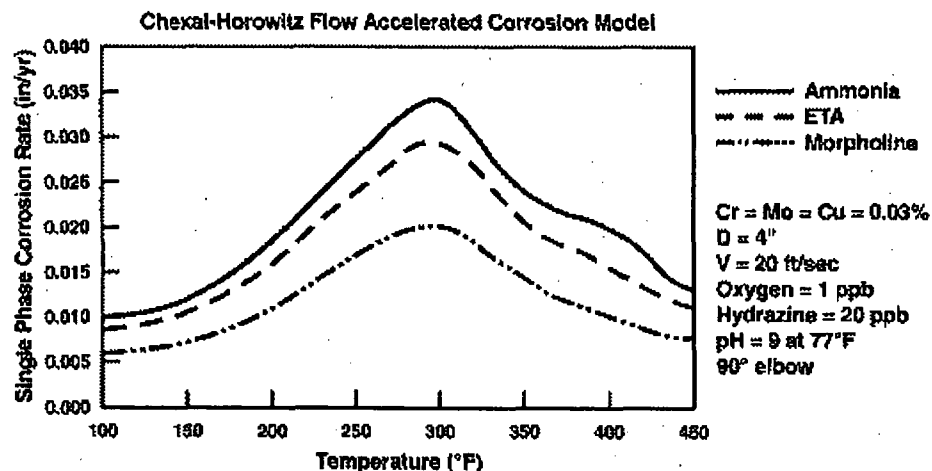


Figure 7-12. Chexal-Horowitz FAC Model, Impact of Using Ammonia or Alternate Amines at a pH of 9 at 77°F (25°C)

Geometry Factor. The geometry factor accounts for the increased mass transfer that takes place in fittings due to increased flow turbulence (e.g. from flow direction changes as in an elbow) versus the mass transfer that occurs in a straight pipe. At the time the development of the Chexal-Horowitz model was started, the only widely recognized geometry factors were those of Keller [7.1]. These values, which were developed through pressure drop considerations and designed to be applied to two-phase flow, were compared to plant data and were found not to be representative of single-phase flow-accelerated corrosion. In view of the lack of other published information, plant data were used to establish the geometric factors.

Additionally, NEI International Research & Development Company, Ltd. in England was asked to employ the method of Poulson [7.24] to investigate single-phase and two-phase geometry factors. Briefly, Poulson's method consists of modeling the flow-accelerated corrosion of steel in water with the corrosion of scaled copper components in an acid ferrous chloride solution. The comparable two-phase steam water simulation is done using an air-acid mixture. The use of this method dramatically increases the corrosion rate and allows rapid, cost-effective testing of a variety of geometries. In this method, the rate of corrosion is

controlled by the reduction of ferric ions which is the cathodic reaction, and copper dissolving as a monovalent copper chloride complex. This method has been tested in single-phase conditions and as expected:

- The corrosion is proportional to the ferric ion concentration and is zero with no ferric ions present.
- Corrosion rate profiles are similar to known mass transfer profiles.
- Peak, plateaus and enhancement factors are the correct function of Reynolds number.
- Actual corrosion rates are close to those predicted from existing mass transfer correlations.

Another innovation in this area was the definition of a component category to cover the straight pipe immediately downstream of a fitting. Separate geometry factors were developed for each situation.

In 1994, hundreds of records of plant inspections were evaluated to refine and improve the geometry factors. These improvements have been incorporated in CHECWORKS version 1.0C and later versions of the code.

The dependence of the predicted FAC rate on the fitting geometry is presented in Figure 7-13.

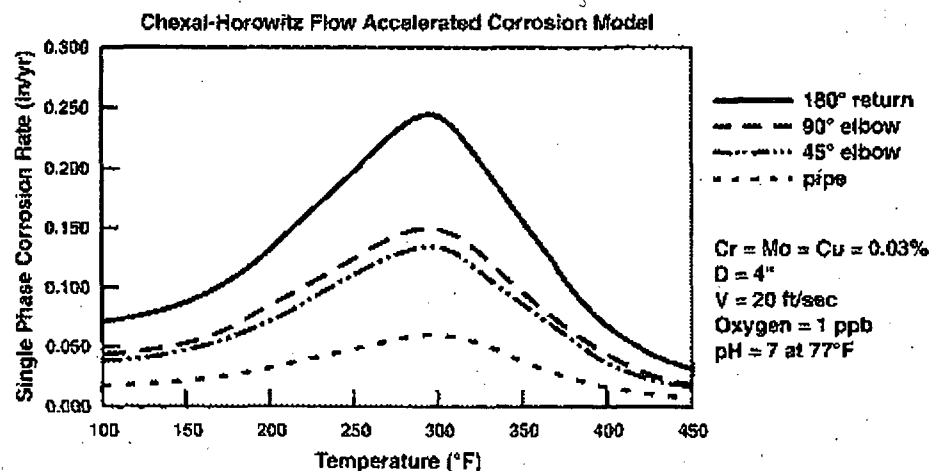


Figure 7-13. Chexal-Horowitz FAC Model, Impact of Fitting Geometry

Void Factor. Two-phase flow adds to the complexities of single-phase flow-accelerated corrosion. To represent the two-phase phenomena, at least one more correlating variable must be added. This variable was chosen to be the void fraction, α . The void fraction is defined as the ratio of the area occupied by the vapor to the total area of the channel. It should be noted that void fraction and quality (the ratio of steam flow rate to the total flow rate) are not equivalent because in general the steam and water phases are moving with different velocities. Also, quality is a mass-based parameter, while the void fraction is an area based quantity.

The void fraction for a component containing a two-phase flow environment is calculated using a void fraction correlation developed by Chexal et al. [7.25]. The key variables needed for determining the void factor are pressure, orientation, total mass flow rates, quality and pipe diameter. When the void fraction is zero, i.e. if the flowing fluid is single-phase liquid, $F_f(\alpha) = 1$ and the model becomes a single-phase flow-accelerated corrosion rate predictor. When the void fraction is one, i.e. there is no liquid present, $F_f(\alpha) = 0$.

The dependence of the predicted FAC rate on the steam quality is presented in Figure 7-14.

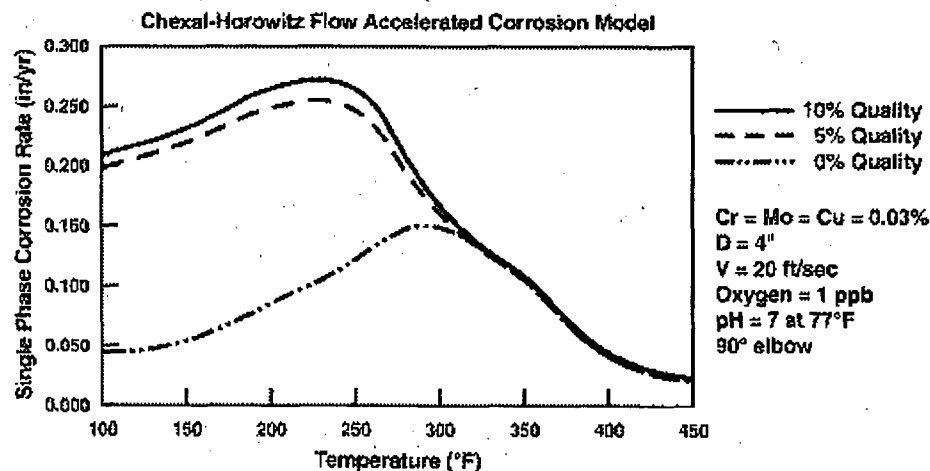


Figure 7-14. Chexal-Horowitz FAC Model, Impact of Steam Quality

Hydrazine factor. Recent work has indicated a strong relationship between the oxidizing reducing potential (ORP) and the rate of FAC. The ORP is related to the amount of dissolved oxygen and the concentration of a reducing agent such as hydrazine. The oxygen dependency is included as the F_4 factor previously discussed. This relationship appears to be most significant in fossil plants that operate at a pH about 9 with and without hydrazine [7.26, 7.27]. In this operating regime, the rate of FAC appears to be greatly reduced when the hydrazine is eliminated.

To fully account for the influence of ORP on the rate of FAC a new factor has been developed. This factor, F_8 has been designed to account for the presence of hydrazine. The dependence of the predicted FAC rate on the hydrazine level is presented in Figure 7-15. The hydrazine factor has been developed to cover the entire range of hydrazine concentrations from 0 ppb (typical of some fossil plants) to about 500 ppb (typical of some Japanese PWRs). This factor has been added to version 1.0F of CHECWORKS.

The FAC rate dependence on hydrazine can be seen in Figure 7-15, below.

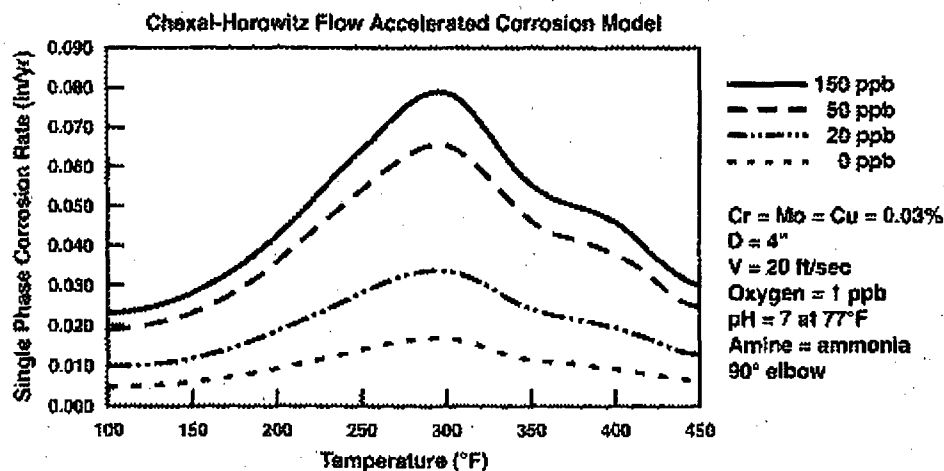


Figure 7-15. Chexal-Horowitz FAC Model, Impact of Hydrazine Concentration

Model Performance Against Laboratory Data

The predictive model was validated by comparing it against all of the available laboratory data from EDF in France and CEGB in England. It should be noted that laboratory data tend to be more accurate than plant data because:

- The initial thickness of the sample is well characterized, and the thickness measurements are typically made with thin layer activation. This is a very precise way of measuring the wall thickness
- The chemistry and flow conditions are well characterized and accurately measured.

The EDF data were taken at the Ciroco Loop at the EDF facility in Les Renardières, France. The bulk of the data were taken in 0.315 inch (8 mm) inside diameter carbon steel tubes. The CEGB data were taken at the CEGB Loop in Leatherhead. The bulk of the data were taken in 0.354 inch (9 mm) inside diameter carbon steel tubes.

Figure 7-16 shows the performance of the Chexal-Horowitz correlation against single-phase laboratory data. As can be seen, the agreement is quite good.

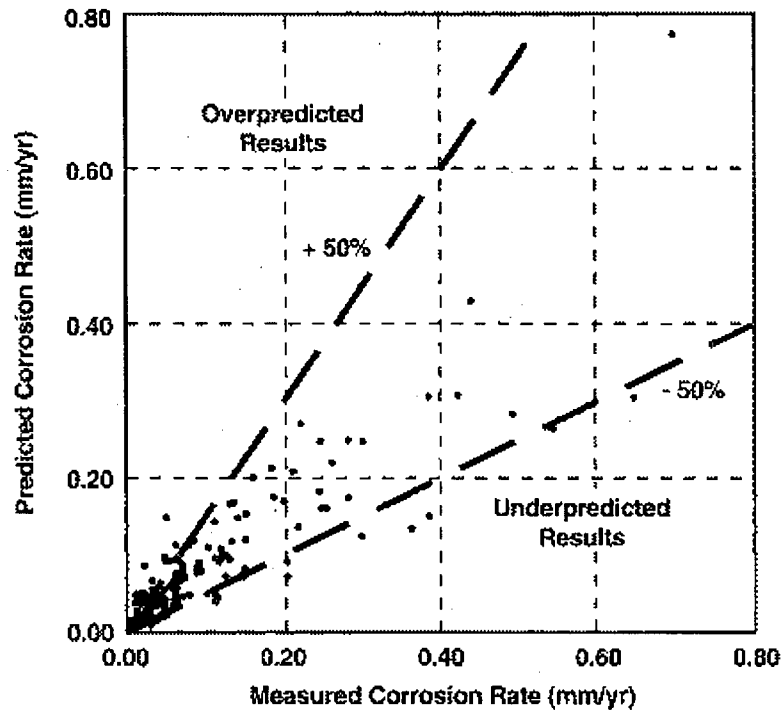


Figure 7-16. Chexal-Horowitz FAC Model, Comparison Against Laboratory Data

Comparison with Plant Data

The purpose of the predictive algorithm is to predict actual plant behavior. To validate the model, data from twenty nuclear plants were used. As mentioned before, plant data are inherently less accurate than laboratory data because of uncertainties in piping operating conditions, and also because of the lack of baseline thickness measurements of the piping components.

In most cases, experience has found that discrepancies between model predictions and plant data results from uncertainties in actual operation of the system and plant, and actual condition of the as-built piping. These uncertainties include:

- The original thickness and thickness profile of the piping components.

- Trace amounts of alloying elements that are present in the piping, but have not been included in the predictions.
- Inaccuracies in the NDE inspection data.
- Actual steam quality of two-phase systems.
- Mistaking other corrosion related damage for FAC (e.g. cavitation or general corrosion during shutdown periods).
- Uncertainties in the actual number of hours or fraction of time that a system or train operates.
- Uncertainties in the plant chemistry history.
- Unknown internal discontinuities within the piping such as counterbore, backing rings, and mismatches with regards to piping fit-up.

However, in spite of these uncertainties, application of the code at operating power plants has repeatedly demonstrated the reliability of the model to identify problem areas needing to be inspected.

Figure 7-17 shows the performance of the Chexal-Horowitz correlation against single and two-phase plant data. As can be seen, the agreement is still quite good.

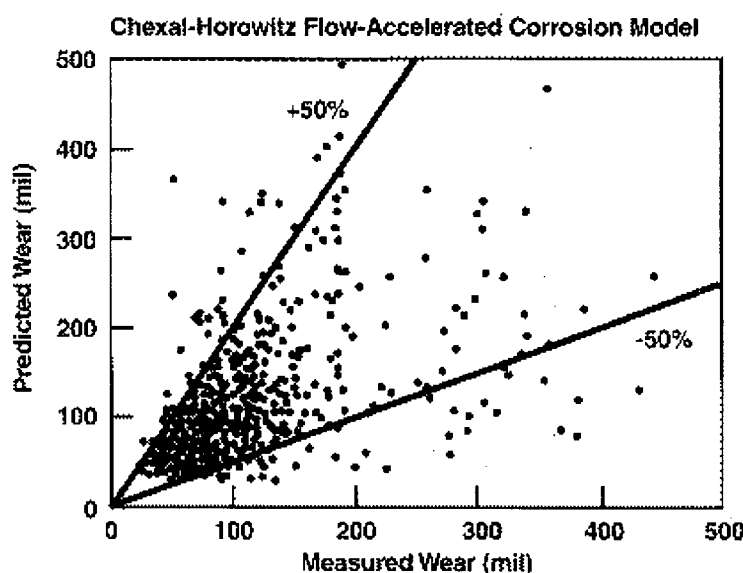


Figure 7-17. Chexal-Horowitz FAC Model, Comparison Against Plant Data